

Dynamic Model of Basic Oxygen Steelmaking Process Based on Multi-zone Reaction Kinetics: Model Derivation and Validation



BAPIN KUMAR ROUT, GEOFF BROOKS, M. AKBAR RHAMDHANI, ZUSHU LI, FRANK N.H. SCHRAMA, and JIANJUN SUN

A multi-zone kinetic model coupled with a dynamic slag generation model was developed for the simulation of hot metal and slag composition during the basic oxygen furnace (BOF) operation. The three reaction zones (i) jet impact zone, (ii) slag–bulk metal zone, (iii) slag–metal–gas emulsion zone were considered for the calculation of overall refining kinetics. In the rate equations, the transient rate parameters were mathematically described as a function of process variables. A micro and macroscopic rate calculation methodology (micro-kinetics and macro-kinetics) were developed to estimate the total refining contributed by the recirculating metal droplets through the slag–metal emulsion zone. The micro-kinetics involves developing the rate equation for individual droplets in the emulsion. The mathematical models for the size distribution of initial droplets, kinetics of simultaneous refining of elements, the residence time in the emulsion, and dynamic interfacial area change were established in the micro-kinetic model. In the macro-kinetics calculation, a droplet generation model was employed and the total amount of refining by emulsion was calculated by summing the refining from the entire population of returning droplets. A dynamic Fe_tO generation model based on oxygen mass balance was developed and coupled with the multi-zone kinetic model. The effect of post-combustion on the evolution of slag and metal composition was investigated. The model was applied to a 200-ton top blowing converter and the simulated value of metal and slag was found to be in good agreement with the measured data. The post-combustion ratio was found to be an important factor in controlling Fe_tO content in the slag and the kinetics of Mn and P in a BOF process.

<https://doi.org/10.1007/s11663-017-1166-7>

© The Minerals, Metals & Materials Society and ASM International 2018

I. INTRODUCTION

THE basic oxygen furnace (BOF) has been a leading route of steel production for more than six decades and become mature in terms of safety, stable operation, and maximization in productivity. However, nowadays it faces different challenges, *e.g.*, strict quality control, minimizing energy cost, maximizing yield, and reducing environmental pollution. Focusing on improving the process by developing fundamental understanding and enabling dynamic correction is the crucial step to optimize

the BOF process. A dynamic model that can explain the changes in the critical process parameters based on the events taking place in the furnace operation is a must-have tool for the operators. It can be a base to develop an automatic control system of the process. Therefore, in the recent years, there has been an increasing amount of literature focusing on developing computer-based dynamic models for the BOF process.^[1–13]

Kattenbelt and Roffel^[9] developed a dynamic model for BOF based on the measured step response of control variables such as oxygen flow rate, lance height, and flux addition. Although the authors discussed the mechanism of decarburization reaction based on the work of droplet generation, the size of droplets, and residence time in the emulsion, no fundamental relationship to include these parameters was employed in this work. Li *et al.*^[12] applied the three-stage decarburization theory and applied three separate equations to simulate the decarburization rate. The rate equations were modified with the bath mixing degree, which was described as a function of dynamic lance height. The rate constants of

BAPIN KUMAR ROUT, GEOFF BROOKS, and M. AKBAR RHAMDHANI are with the Faculty of Science, Engineering and Technology, Swinburne University of Technology, Hawthorn, VIC 3122. Contact e-mail: brout@swin.edu.au ZUSHU LI is with the WMG, University of Warwick, Coventry, CV4 7AL, UK. FRANK N.H. SCHRAMA and JIANJUN SUN are with Tata Steel, Building 4H16, PO Box 10000, 1970 CA, IJmuiden, Netherlands.

Manuscript submitted June 23, 2017.

Article published online January 8, 2018.

the equations were derived by fitting the data from 67 heats. Similar to Kattenbelt and Roffel,^[9] the dynamic model developed by Li *et al.*, cannot provide a physical insight into the BOF process due to the empiricism involved in deriving the rate parameters.

Understanding that the BOF process rarely attains thermodynamic equilibrium,^[14] the principle of chemical kinetics has appealed to many researchers in quantitative prediction of the refining rates. Several researchers^[6,7,10] have applied the “coupled reaction mechanism” developed by Robertson and colleagues^[15] to simulate the slag–metal reactions. Pahlevani *et al.*^[6] employed the coupled reaction mechanism in a single-zone kinetic model with the flux dissolution model to simulate the BOF refining reaction. Ogasawara *et al.*^[7] constructed a dynamic model for dephosphorization by combining coupled reaction model with a dynamic Fe₂O generation model. An oxygen balance method combined with the off-gas data was used to predict Fe₂O in the slag during the blow. In the model built by Lytvynuk *et al.*,^[10] the coupled reaction model was combined with the thermodynamics and kinetics of involved phases (interfacial surface of iron melt and slag) in one reaction zone to simulate the BOF process. Scrap melting model and flux dissolution model were included in the simulation. The simulated behavior of metal and slag compositions by the model was validated with the industrial converters of different sizes.

While the above dynamic models based on coupled reaction model found some success in simulating the slag–metal reactions, the biggest challenge in this type of approach is to quantify the rate parameters, especially the slag–metal interfacial area that is a strong function of dynamic process conditions. Due to lack of fundamental basis to quantify rate parameters such as interfacial area, the above kinetic models employed

fitting parameters in the model which are derived from the plant-specific data.^[8,10–12]

The major reactions of BOF process are schematically presented in Figure 1. Based on the difference of reaction environments and mass transfer conditions, the primary reactions zones are divided as follows: (i) jet impact area where the direct reaction between oxygen gas and melt takes place in an extremely hot environment, (ii) slag–metal emulsion phase, where the reaction between metal drops and slag takes place, and (iii) slag–bulk metal zone, where a permanent phase contact between the slag and bulk metal is realized. Kinetic parameters of the reactions in a zone can be described as a function of interfacial area, temperature, and physicochemical nature of phase interactions. Brooks *et al.*^[16] argued that the use of simple first-order rate is not appropriate for modeling the BOF process and a transient kinetics approach is necessary to describe the multi-phase heterogeneous reactions. A recent publication by Hewage *et al.*^[17] by analyzing the IMPHOS pilot plant data^[18] showed that a single zone with the first-order rate equation may be applicable for the simple reaction like Si oxidation, but the compositional change of P, Mn, and C cannot be explained by a simple first-order kinetics with constant rate parameters. Similarly, Rout *et al.*^[19] analyzed the rate of dephosphorization for a 200-ton converter data and found that the kinetics of dephosphorization depends on the rate at which the droplets refined in the emulsion and therefore considering the interfacial area at the bulk metal and the slag, cannot simply explain the dephosphorization behavior.

Several other researchers developed multi-zone models for BOF process by dividing the converter into several reaction zones.^[2,4,5] Jalkanen and Holappa^[2] developed a physicochemical model for the BOF process

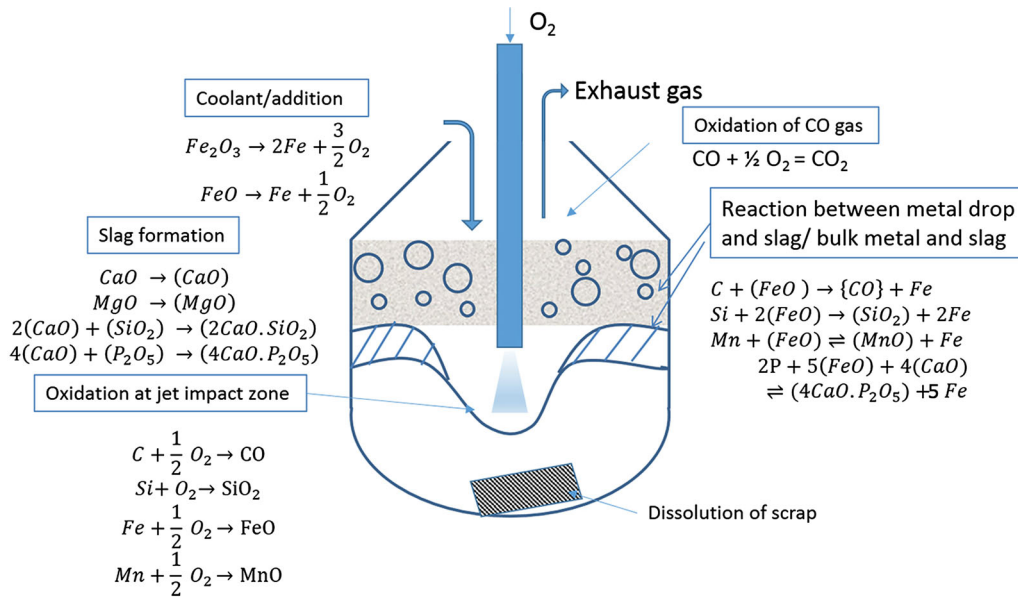


Fig. 1—Schematic representation of reactions in BOF converter.

by considering the reaction in three different zones of the converter. In the computational model, the three reaction zones were replaced by a generalized reaction zone and the distribution of oxygen among the various impurities was simulated by their individual reaction affinities expressed by Gibb's reaction energies. The model uses several fixed parameters derived from the plant data and the simulated results are only able to capture the qualitative representation of metal and slag compositions. Dogan *et al.*^[6] developed a comprehensive model for decarburization by considering the refining of C in the jet impact and the emulsion zone. The theory of bloated drops in the emulsion and the residence time of the metal drops are successfully incorporated in the model, and the model C prediction was found to be consistent with the industrial converter data. However, no FeO prediction model was employed in their study. Sarkar *et al.*^[8] dynamic model focused on

developing a kinetic treatment to the reactions in the emulsion zone. The Gibb's free energy minimization was applied for simultaneous oxidation kinetics of elements in the metal droplet. In common with Dogan *et al.*, the model was able to incorporate the phenomena of droplet generation, bloating, and residence time model in the overall kinetic equation. However, the model prediction of reactions other than C removal was poor, particularly the reversion of Mn and P. In a more recent study by Sasaki and colleagues,^[13] a three-zone kinetic model for industrial BOF operation was employed to predict the metal and slag composition successfully. However, the key model details are not available in the open literature.

The present work has been undertaken to develop a dynamic model for BOF process using the multi-zone kinetic theory. The model attempts to capture most of the physiochemical phenomena of the process by considering three primary refining zones commonly observed in a top blowing process. The ejection of droplets, phenomena of droplet "bloating" due to nucleation of CO gas, and detailed reaction kinetics of droplets for a multicomponent system in the emulsion phase were successfully taken into account in the dynamic model. The overall model was validated with the measured data of a 200-ton industrial converter. The details of the development of the global model and its validation with the industrial data are presented in this

Table I. Impurities Removed in Different Zones of a BOF Converter

Reaction Zones	Impurities Removed
Jet impact (hot spot)	C, Si, Mn
Slag–bulk metal	C, Si, Mn, and P
Slag–metal emulsion	C, Si, Mn, and P

Table II. Rate Equations in Three Different Zones of the Converter

Reaction Zones	Rate Equations	Model Parameters
Jet impact zone (gas–metal)	$\left. \frac{d(W_m C_{jm})}{dt} \right _{iz} = -A_{iz} k_m^{gm} \rho_m (C_{jm} - C_{ji}^{gm}),$ $j = \text{Si, Mn, P and } C \leq 0.3 \text{ wt pct} \quad [1]$ <p>For C oxidation, $C > 0.3$ wt pct: $\left(\frac{dW_c}{dt} \right)_{iz}$</p> $= \left(\frac{dW_c}{dt} \right)_{iz}^{CO_2} + \left(\frac{dW_c}{dt} \right)_{iz}^{O_2} \quad [2]$ $\left(\frac{dW_c}{dt} \right)_{iz}^{CO_2} = -100 \times M_C A_{iz} k_a P_{CO_2}^b \quad [3]$ $\left(\frac{dW_c}{dt} \right)_{iz}^{O_2} = -200 \times M_C A_{iz} k_g (1 + P_{O_2}^b) \quad [4]$	Jet impact area: A_{iz} , gas/metal interface concentration C_{ji}^{gm} , mass transfer coefficients: k_m^{gm} , k_g , k_a
Slag–bulk metal (slag–metal)	$\left. \frac{d(W_m C_{jm})}{dt} \right _{sm} = -A_{sm} k_m^{sm} \rho_m (C_{jm} - C_{ji}^{sm}) \quad [5]$	Slag–bulk metal area: A_{sm} , slag/metal interfacial concentration C_{ji}^{sm} , mass transfer coefficient k_m^{sm}
Slag–metal emulsion (slag–metal drops)	<p>Rate of mass transfer between metal drops and slag:</p> $\left. \frac{d(m_d C_{jd})}{dt} \right _{em} = -A_d k_d^{em} \rho_m (C_{jd} - C_{ji}^{em}) \quad [6]$ <p>Rate of refining of bulk metal by emulsion:</p> $\left. \frac{d(W_m C_{jm})}{dt} \right _{em} = - \frac{W_{jm}^{eject,t} - W_{jm}^{return,t}}{\Delta t} \quad [7]$ $W_{jm}^{eject,t} = \left(\sum_{p=1}^P (R_{B,T})_p \times \Delta t \right) \times \frac{C_{jm}^c}{100} \quad [8]$ $W_{jm}^{return,t} = \sum_{p=1}^P N_p^{return,t} \times \frac{(C_{id}^{return,t} m_d^{return,t})_p}{100} \quad [9]$ $N_p^{return,t} = N_p^{eject,t-t_{res}} = \frac{W_{d,p}^{t-t_{res}}}{\bar{m}_{d,p}} \quad [10]$	Interfacial area of droplet A_d , residence time of drops in emulsion t_{res} , mass transfer coefficient k_d^{em} , droplet generation rate $R_{B,T}$ metal droplet concentration C_{jd} interfacial concentration at metal drop/slag interface C_{ji}^{em} , $\bar{m}_{d,p}$ average droplet mass of size class p (p droplet size class, P total number of classes in the droplet size spectrum; Please refer Section I–A–i–v)

paper, while the kinetic models of decarburization and demanganisation are described in separate papers.^[20,21]

II. MODEL CONCEPTS AND MATHEMATICAL FORMULATION

Mathematical treatment to the kinetics of the reactions occurring in each reaction zone has been developed to simulate the overall refining rate of liquid metal. Table I shows reaction zones considered for refining of individual impurities in the converter. It is well understood that the removal of phosphorus needs a basic slag due to thermodynamic instability of P_2O_5 at steelmaking temperature. Due to the large impact force exerted by the gas jet on the bath surface, the slag beneath the jet is entirely pushed away from the jet impact zone to the periphery region and the oxygen gas directly reacts with the hot metal.^[22] Therefore P removal in the jet impact zone is ignored in this study.

The rate equations that describe the refining in the different zones of the converter and the transient kinetic parameters are listed in Table II.

The overall rate of refining can be described by the following equation:

$$\left. \frac{d(W_m C_{jm})}{dt} \right|_{\text{overall}} = \left. \frac{d(W_m C_{jm})}{dt} \right|_{\text{iz}} + \left. \frac{d(W_m C_{jm})}{dt} \right|_{\text{sm}} + \left. \frac{d(W_m C_{jm})}{dt} \right|_{\text{em}} \quad [11]$$

A. Jet Impact Zone

The kinetics of oxidation of Si, Mn in jet impact zone was assumed to be controlled by mass transport in the liquid phase. It is due to rapid dissolution of oxygen in the melt as a result of high temperature prevailing in the hot spot region. The mass transfer coefficient of Si, Mn (k_{gm}^m) in the metal phase has been calculated as a function of stirring energy and geometrical parameters of the furnace (see Appendix A.1).^[23] The interfacial concentration C_{im} has been calculated assuming dynamic equilibrium between the reactants and products at the gas/metal interface. The rate parameters for carbon oxidation (k_a and k_g in Eqs. [3] and [4]) have been simulated by mixed controlled kinetics, including the gas phase mass transfer and chemical reaction kinetics as rate determining steps.^[24] Below a critical level of C, the rate of decarburization was assumed to be controlled by carbon diffusion in metal phase.^[25,26] It has been reported that the value of critical carbon may lie between 0.3 and 0.8 wt pct depending on the oxygen flow rate. In the present study, a fixed value of critical carbon of 0.3 wt pct was considered.^[25,26] The detail mathematical model for C, Si, and Mn oxidation kinetics in jet impact zone can be found elsewhere.^[20,21,27]

The interfacial area was assumed to be the area of the cavity created by the top jet. The surface area of the jet impact was considered to be paraboloid in shape^[28] and

was calculated as a function of lance height and oxygen flow rate.

$$A_{\text{cav}} = \int_0^r 2\pi r_{\text{cav}} \left(1 + \left(\frac{dh}{dr} \right)^2 \right) dr, \quad [12]$$

where A_{cav} is the area of the individual cavity; h is the height; and r_{cav} is the radius of the cavity. The analytical solution to Eq. [12] can be expressed as

$$A_{\text{cav}} = \frac{\pi r_{\text{cav}}^4}{6h^2} \left[\left(1 + \frac{4h^2}{r_{\text{cav}}^2} \right)^{3/2} - 1 \right]. \quad [13]$$

The height and radius of the cavity were calculated by using the dimensionless correlations suggested by Korla and Lange.^[29] The detailed calculation regarding the cavity dimensions is given in Appendix A.2.

It has been observed that the jet cavity formed by each nozzle does not overlap each other when the jet angle exceeds 10 deg. Therefore, in the present work (nozzle angle of 17.5 deg), the total cavity area has been estimated by multiplying individual cavity area by the number of nozzles in the lance tip.

$$A_{\text{iz}} = n_n A_{\text{cav}}. \quad [14]$$

Here n_n is the number of nozzles and A_{iz} is the total surface area of jet impact. The change of cavity shape due to surface oscillation was neglected since it exerts little effect on the final area calculation.^[28] The rate Eqs. [1] through [4], described in Table II, have been employed to determine the weight of refining of C, Si, Mn in the jet impact area.

B. Emulsion Zone

Many researchers suggested that rapid refining of hot metal in a BOF process proceed *via* the formation of slag–metal–gas emulsion zone.^[18,30,31] However, the proportion of refining brought by emulsion zone to the overall bulk metal refining is not clear from the past studies. The mechanism of refining of hot metal by the metal droplet circulation in emulsion zone is schematically illustrated in Figure 2. The droplets ejected from the liquid metal, initially carry the melt concentration and once it remains in contact with the oxidizing slag, refining of impurity elements begin to take place. From the laboratory scale study of droplets, it has been observed that the formation of CO either inside or on the surface of the drops as a result of the decarburisation reaction makes the droplet buoyant and increase the residence time in the emulsion. Fruehan and co-workers^[31] were able to capture the phenomena of “bloating” of a metal droplet in a steelmaking type of slag by X-ray fluoroscopy technique. The important aspect of “bloating” is that it increases the residence time of metal droplets in the emulsion, which allows the metal droplets to react with slag for a long period. The continuous creation of large surface area by the formation of small-sized drops and high reaction time in the emulsion is believed to be a prominent mechanism of BOF refining process.^[18,30,31]

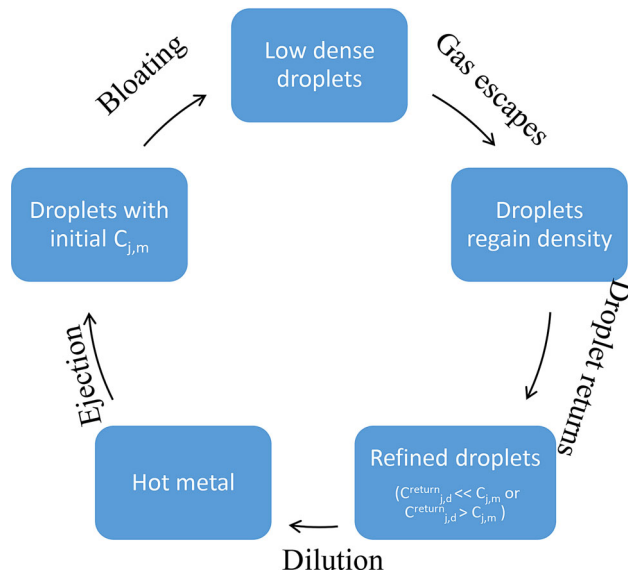


Fig. 2—Schematic representation of the refining mechanism in the emulsion zone.

The process of refining by emulsion can be visualized in two stages: refining of a single droplet and overall refining by all the droplets. Note that the droplets present in the emulsion at a given blowing time can undergo different physicochemical processes depending on their time of the ejection, initial size, and residence time. The mathematical treatment to model the refining of bulk metal by the emulsion zone has been divided into two stages:

- (1) Rate of refining between an individual metal droplet and slag—micro-kinetics approach
- (2) Overall rate of refining by the entire population of the metal droplets—macro-kinetics approach.

1. Micro-kinetics of droplet refining in emulsion

The rate equation for refining of elements of a single droplet during the time of residence inside the emulsion can be presented by a first-order rate law as presented in Eq. [6] in Table II. The mathematical treatment to simulate the transient rate parameters such as interfacial area, mass transfer coefficient, and interface concentration in the rate equation is presented in the following sections.

a. Simultaneous refining kinetics of impurities. The kinetic model suggested by Brooks *et al.*,^[32] which uses surface renewal method of carbon diffusion, has been applied to simulate the rate of decarburisation of droplets in the emulsion zone. This approach has been found to be mathematically reliable in connecting the bloating behavior of droplets to the overall decarburisation kinetics in the emulsion zone. As suggested by Dogan *et al.*,^[6] since there are plenty of oxygen available in the system, the rate of CO formation may be rapid and carbon diffusion can be the rate controlling step for a bloated droplet. While there is no collective agreement regarding the rate determining step of the

decarburisation kinetics of droplet, the authors have used the above-mentioned approach to connect the bloating phenomena of the droplets to the overall refining of the BOF process. However, further work is necessary to establish an accurate kinetic model for decarburisation.

The fundamental understanding of the simultaneous mass transfer of Si, C, Mn, and P across the boundary between the metal droplet and slag interface is limited in the steelmaking literature. There are only a few laboratory scale studies on the kinetics of Fe-C-S,^[33] Fe-C-P,^[34,35] Fe-C-P-S,^[36] and Fe-C-Si-Mn.^[37] The following observations regarding the kinetics of metal droplets in the slag can be made from the past studies:

- (1) The rate of C removal slows down in the presence of Si and Mn in the droplet.^[37]
- (2) The rate of phosphorus removal is very rapid in the presence of C in the droplet. Phosphorus in the droplet reaches the equilibrium concentration within a few seconds after it enters into the oxidizing slag.^[34–36]
- (3) Internal nucleation of CO gas increases the kinetics of P transfer and an increase of S level in the droplet influences the CO formation rate.^[38]

Based on these observations, a mechanism of the simultaneous kinetics of C, Si, Mn, and P at droplet and slag interface was proposed. According to the proposed reaction mechanism, shown in Figure 3, the oxidation kinetics of Si, P, and Mn proceeds at rapid rate and approaches the equilibrium within a few seconds after the metal drops enters into the emulsion phase. Gaye and Riboud^[34] and Geiger and colleagues^[35] and more recently Gu *et al.*^[36] observed that the kinetics of P for Fe-C-P is very rapid and attains the equilibrium value in 10 seconds. It is further proposed that the quick formation of surface active oxides like SiO₂ and P₂O₅ slows down the kinetics of decarburisation by blocking the reaction sites for C and FeO reaction. The detail calculation of mass transfer coefficient of carbon in the presence of surface active oxides is discussed elsewhere.^[20] Carbon refining in a bloated droplet continues until it attains the equilibrium and once the CO gas escapes, the dense and refined drops return to the metal bath.

b. Mass transfer coefficient. Several researchers suggested that Higbie's penetration theory can be used to model the mass transfer coefficient of decarburization rate of a moving metal droplet in the slag-metal emulsion.^[32,39] According to Higbie's theory, it has been assumed that when a metal droplet moves (ascends, descends, or floats) in the slag-metal emulsion domain, the slag packets are brought into contact by turbulent eddy and undergo unsteady state diffusion or penetration by the transferred species during its contact time. For a bubble-agitated stirring system, the calculation of contact time is uncertain, and there is apparently no reliable method available to estimate it. However, for a simple geometry like a spherical droplet which ascends or descends in the slag layer, the contact

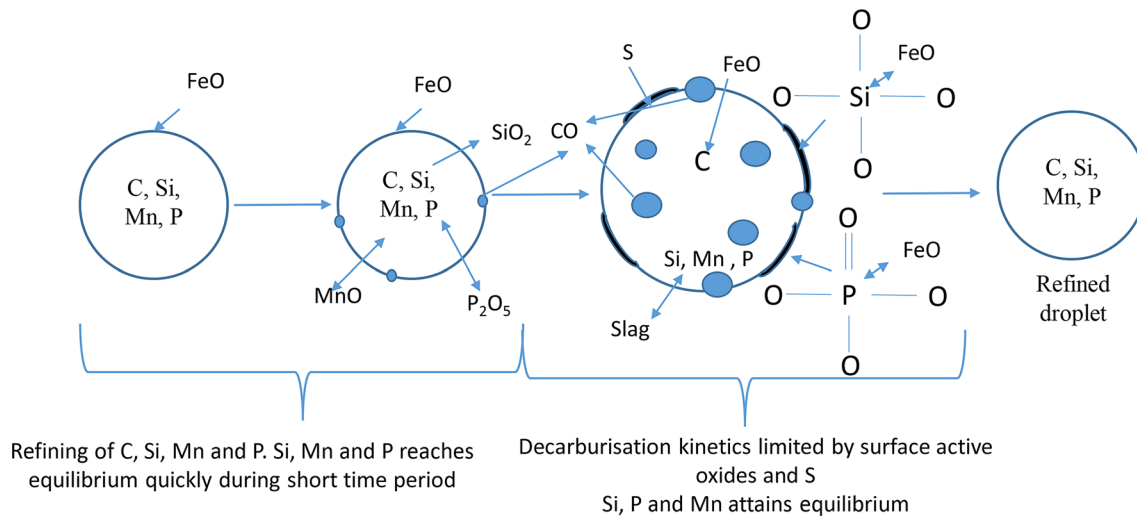


Fig. 3—Proposed refining mechanism of metal droplets in the slag–metal emulsion.

time can be assumed to be the ratio of diameter to the velocity of the spherical bubble.^[39] The mass transfer coefficient in the metal phase can be calculated as follows:

$$k_{jm}^d = 2 \times \sqrt{\frac{D_j}{\pi t_c}} = 2 \times \sqrt{\frac{D_j u}{\pi d_p}}, \quad [15]$$

where k_{jm}^d is the mass transfer coefficient in metal phase; D_j is the diffusion coefficient of the j th element in metal drop; t_c is the contact time of the slag packet with the metal drop; u is the velocity of the drop; and d_p is the average diameter of the drop corresponding to the size class p . The diffusion coefficient of C, Si, Mn, and P has been taken from the reported data of solute diffusivity values of elements in the liquid Fe–C alloy at 1873 K (see Table IV). Further, the temperature and viscosity effect on mass diffusivity was taken into account by applying the Stokes–Einstein equation.

$$D_T = D_{1873} \left(\frac{T}{1873} \right) \times \left(\frac{\mu_{m,1873}}{\mu_{m,T}} \right), \quad [16]$$

where D_T is the diffusivity at temperature T (m^2/s); D_{1873} is the diffusivity of species at $T = 1873$ K (m^2/s); T is the temperature (K); $\mu_{m,1873}$ and $\mu_{m,T}$ are the viscosity of hot metal at 1873 K and T , respectively. In the present work, the effect of temperature on viscosity has been neglected.

On the slag side, it is assumed that the metal droplet is a rigid sphere with the stream of slag surrounding it. Due to high Schmidt number prevailing in steelmaking systems, the boundary layer is considered laminar and the effect of turbulence on mass transfer coefficient can be neglected. According to Oeters,^[40] the mass transfer coefficient in slag phase (k_s^d) can be determined by the following equation:

$$Sh = 2 + 0.6Re^{1/2}Sc^{1/3}, \quad [17]$$

where Sh is the Sherwood number; Re is the Reynolds number; and Sc is the Schmidt number. The ion

diffusivity in slag, D_{slag} (in Sherwood number calculation), was taken to be $5 \times 10^{-10} m^2/s$.^[40]

Liquid phase mass transfer control has been assumed for decarburization reaction in the droplets. However, the reactions of Si, Mn, and P were assumed to be controlled by both mass transfers in metal and the slag. The overall mass transfer coefficient (k_d^{em}) of the metal droplet in slag, assuming a mixed transport controlled reaction kinetics can be written as^[41]

$$\frac{1}{k_d^{em}} = \frac{1}{k_{jm}^d} + \frac{\rho_m}{k_s^d \rho_s L_j}. \quad [18]$$

Here k_{jm}^d and k_s^d are the mass transfer coefficient in metal and slag phase, respectively. ρ_m and ρ_s are the densities of metal and slag, respectively. L_j is the equilibrium distribution ratio between the slag and metal droplet.

c. Interfacial concentration. The instantaneous equilibrium between the reactants and products has been assumed at the metal drop and slag interface. Slag–bulk metal equilibria were applied to estimate the equilibrium concentration of each component at the metal drop interface. The equilibrium concentration of carbon was determined by calculating the activity coefficient, concentration, and the equilibrium value. It has been observed that both temperature and composition have strong effect on the activity coefficient of C, and therefore a polynomial equation of f_c as a function of both C and temperature proposed by Chou *et al.*^[25] has been used in this work. The Raoultian activity of iron oxide has been simulated as a function of slag composition and temperature by applying regular solution model.^[42] In the case of Si, Mn, and P, the equilibrium distribution ratio as a function of the composition and the temperature has been used for the estimation of interfacial concentration

$$[\text{wt pct } C_{ji}] = \frac{(\text{wt pct } C_j)}{L_j}, \quad [19]$$

where $[C_{ji}]$ is the concentration (wt pct) at the slag/metal interface; (C_i) is the concentration (wt pct) in the slag; and L_j is the equilibrium partition ratio between the metal and slag.

The experimental data reported by Narita *et al.*,^[43] were used to develop a linear correlation of interfacial Si concentration between the metal and slag as a function of slag FeO (< 40 wt pct). The equilibrium distribution ratio suggested by Suito and Inoue,^[44] which is valid for CaO-SiO₂-FeO type slag with MnO concentration varying up to 16 wt pct was used to calculate the interfacial manganese concentration. Cicutti *et al.*^[45] reported that the equilibrium value of P predicted by the regular solution model agrees well with the oxidation and reversion behavior of P in an industrial furnace. Thus, in the present work, the P partition ratio was determined by regular solution model. The evaluation of interfacial concentration at the metal drop and slag boundary for various impurities (C, Si, Mn, and P) is illustrated in Table III. The equilibrium distribution ratio models are illustrated in Appendix A.3.

d. Dynamic interfacial area of the droplet. The change in the area and volume of the metal droplet due to bloating phenomena has been estimated by an empirical correlation for density variation as a function of decarburization rate, suggested by Brooks *et al.*,^[32] based on the experimental measurements by Molloseau and Fruehan^[32]:

$$\rho_d = \begin{cases} \rho_{d0} \frac{r_c^*}{r_c}, & r_c > r_c^*, \\ \rho_{d0}, & r_c \leq r_c^*, \end{cases} \quad [20]$$

where ρ_{d0} is the initial droplet density before bloating; ρ_d is the droplet density during the decarburisation reaction; r_c is the decarburisation rate; and r_c^* is the critical decarburisation rate, which is empirically correlated with the iron oxide concentration in the slag. The critical decarburisation rate (r_c^*) has been evaluated by the following empirical relationship.^[37]

$$r_c^* = \begin{cases} 2.86 \times 10^{-4} \times 20, & \text{wt pct FeO} > 20, \\ 2.86 \times 10^{-4} \times (\text{wt pct FeO}), & \text{wt pct FeO} \leq 20. \end{cases} \quad [21]$$

Assuming the droplets are spherical in shape, the following equations have been used to calculate the evolution of the surface area of a droplet as a function of residence time in the emulsion phase:

$$d_p(t) = \left(\frac{6}{\pi} \times \frac{m_d}{\rho_d(t)} \right)^{1/3}, \quad [22]$$

$$A_d(t) = \pi \times d_p(t)^2, \quad [23]$$

where m_d is the mass of the ejected droplet, and $d_p(t)$ and $\rho_d(t)$ are the time varying diameter and density of droplet in the emulsion.

e. Size distribution of droplets. The size of ejected droplets can exert significant influence on reaction kinetics in the emulsion.^[18] Therefore, a size distribution model was applied to calculate the diameter of droplets at the place of their birth from the bath. The model assumes that the size distribution of metal droplets follows Rosin–Rammler–Sperling (RRS) distribution function.^[45,46]

$$R_s = 100e^{[-(\frac{d}{d'})^n]} \text{ in wt pct}, \quad [24]$$

where R_s is the quantity of screen oversized with diameter d . n and d' are parameters of distribution function, which represent homogeneity of distribution and the measure of fineness, respectively.

The granules of metal droplets collected from the emulsion by Cicutti *et al.*^[45] was found to vary between 2.3×10^{-4} and 3.35×10^{-3} m. In this work, the similar droplet size spectrum has been used to determine the

Table III. Estimation of Interfacial Concentration at Slag–Metal Interface

Reactions	Interface Concentration at Slag/Metal Phase Boundary	Methods
Carbon [C] + (FeO) = {CO} + [Fe]	$[\text{pct C}]_{\text{eq}} = \frac{P_{\text{CO}} \times a_{\text{Fe}}}{f_c \times a_{\text{FeO}} \times K_c}$	$P_{\text{CO}} 1.5 \times 10^5$ Pa, $a_{\text{Fe}} = 1$, f_c empirical correlation, ^[25] a_{FeO} regular solution model, ^[39] equilibrium constant: $\log(K_c) = 5.096 - \frac{5730}{T_m}$
Silicon [Si] + (FeO) = (SiO ₂) + [Fe]	$[\text{pct Si}]_i = L_{\text{Si}}^* \times [\text{pct Si}]$	L_{Si}^* : Narita <i>et al.</i> ^[41]
Manganese [Mn] + (FeO) = (MnO) + [Fe]	$[\text{pct Mn}]_i = \frac{(\text{pct Mn})}{L_{\text{Mn}}}$	L_{Mn} : Suito <i>et al.</i> ^[42]
Phosphorus 2[P] + 5(FeO) = (P ₂ O ₅) + 5[Fe]	$[\text{pct P}]_i = \frac{(\text{pct P})}{L_p}$	L_p : regular solution model ^[39]

initial size distribution of ejected droplets. The total range of droplet size has been divided into ten classes with a mean diameter of d_p for each size class. The average diameter increment between two adjacent classes was taken to be 3.12×10^{-4} m. The proportion of droplet weight $W_{d,p}$ corresponding to class p was obtained by applying the RRS distribution function as follows:

$$W_{d,p} = W_{d,\text{total}} \left(\exp \left[- \left(\frac{d_{p+1}}{d'} \right)^n \right] - \exp \left[- \left(\frac{d_p}{d'} \right)^n \right] \right), \quad [25]$$

where $W_{d,\text{total}}$ is the total number of droplets ejected at a time interval of Δt which has been calculated by Eq. [26]:

$$W_{d,\text{total}} = R_{B,T} \times \Delta t, \quad [26]$$

where $R_{B,T}$ is the modified droplet generation rate (kg/s), defined by author's previous work^[45]:

$$\frac{R_{B,T}}{F_{G,T}} = \frac{(N_{B,T})^{3.2}}{[2.6 \times 10^6 + 2.0 \times 10^{-4} (N_{B,T})^{12}]^{0.2}}, \quad [27]$$

where $F_{G,T}$ and $N_{B,T}$ are the temperature-corrected volumetric flow rate and modified blowing number, respectively, and $R_{B,T}$ is the amount of droplet generated per volume of gas. The detail calculation of temperature modified blowing number ($N_{B,T}$) and gas flow rate ($F_{G,T}$) can be found elsewhere.^[47]

The parameters of the distribution function n and d' were chosen such a way that about 95 pct of the particles lie between 2.3×10^{-4} and 3.35×10^{-3} m. By using the non-linear least square fitting, the values of n and d' are estimated to be 1.75 and 1.26, respectively. The parameters in the RRS distribution function presented here may not be universal as the value of d' , is a function of blowing conditions.^[46,48] The present value of n falls in the same range (1.44 ± 0.43) suggested by Subagyo *et al.*^[48]

f. Residence time of the droplets. The mathematical model for the residence time of the metal droplets was based on the principle of ballistic motion, as proposed by Brooks *et al.*^[32] The trajectory of a droplet in both vertical and horizontal directions was calculated by the force balance method with taking into account the dynamic change in density under the influence of bloating. Thus, the decarburisation rate was coupled with the equation of motion to estimate the density change in the emulsion. In the present model, it has been assumed that the droplets are ejected into the emulsion with a certain angle with respect to the melt surface. The following force balance equations have been solved in a two-dimensional coordinate (r, z) to determine the trajectory of a metal droplet:

Force balance along the vertical direction (z -axis):

$$\rho_d V_d \frac{du_z}{dt} = F_B - F_G - F_{D,z} - F_{A,z}. \quad [28]$$

Force balance along the horizontal direction (r -axis):

$$\rho_d V_d \frac{du_r}{dt} = -F_{D,r} - F_{A,r}, \quad [29]$$

where u_z and u_r are the velocity of the drop in z and r directions. The forces $F_B, F_G, F_{D,z}, F_{A,z}$ are buoyancy force, gravitational force, drag force, and added mass force, respectively. Assuming the droplets to be sphere of diameter d_p , the motion of the droplets can be described by the following differential equations:

$$\frac{du_z}{dt} = \frac{2(\rho_s - \rho_d)g}{\rho_s + 2\rho_d} - \frac{\rho_s C_{D,z} A_d}{(\rho_s + 2\rho_d) V_d} u_z^2, \quad [30]$$

$$\frac{du_r}{dt} = - \frac{\rho_s C_{D,r} A_d}{(\rho_s + 2\rho_d) V_d} u_r^2. \quad [31]$$

The drag coefficient $C_{D,z}$ and $C_{D,r}$ in both z and r directions are calculated as a function of Reynolds number.

The initial velocity at the place of birth of the droplet was calculated by applying energy conservation principle suggested by Subagyo *et al.*^[49]:

$$\frac{E_{kd}}{E_{kg}} = 0.00143 N_{B,T}^{0.7}, \quad [32]$$

where E_{kd} is the total kinetic energy absorbed by the droplets by the blowing gas per unit time and E_{kg} is the amount of energy created by the blowing gas per time. The equation of motion of droplet in both horizontal and vertical directions described by Eqs. [29] through [31] with Eqs. [20] and [21] has been solved simultaneously to determine the trajectory and residence time of the bloated droplets. The residence time model determines the total time the droplet resides in the emulsion as a function of initial size, ejection angle, initial velocity, and the slag properties.

g. Temperature at metal drop–slag interface. During the oxygen blowing process, the metal droplets are ejected from a localized superheated zone underneath the oxygen jet. Doh *et al.*,^[50] by coupling chemical reaction of post-combustion with computational fluid dynamics, reported that the maximum temperature of the flame front (as a result of post-combustion reaction) is located near to the bath surface. Since the metal drops are ejected from the jet impact area, the temperature of the droplet interface is expected to experience higher temperature than the bulk melt. During the flight time of drops in the emulsion, a gradual decrease in temperature can be expected due to heat dissipation to the surrounding. Since temperature exerts a significant effect on the mass transfer coefficient and the equilibrium concentration at the reaction interface, a model has been proposed to estimate the interfacial temperature of the metal droplet in slag. It was assumed that the metal droplets are rigid spheres and are more likely to exhibit hot spot temperature at the time of ejection. According to Chao,^[51] the surface temperature of a spherical metal drop having an initial temperature, T_0 and a uniform temperature of T_∞ , when it enters inside the emulsion, can be calculated as follows:

Table IV. Thermal Properties of Steel and Slag Used in the Model for the Calculation of Surface Temperature of Metal Droplet

	Steel	Slag			
		FeO	SiO ₂	CaO	MnO
Heat capacity (J/kg K) ^[52]	821	947	1429.5	928	854.5
Thermal conductivity (W/m K)	40 ^[53]	1.7 ^[54]			

$$T_{\text{drop}} = T_0 + \frac{T_0 - T_\infty}{1 + \beta}, \quad [33]$$

$$\beta = \left(\frac{\lambda_m C_{p,m} \rho_m}{\lambda_s C_{p,s} \rho_s} \right)^{1/2}, \quad [34]$$

where λ is the conductivity (W/m K) and C_p is the heat capacity (J/kg). The subscript m, s corresponds to hot metal and slag. T_{drop} , T_0 , and T_∞ represent the temperature at the droplet interface in the emulsion, temperature of the droplet at the time of ejection, and the emulsion temperature, respectively.

Here we assumed $T_0 = T_{iz}$ and $T_\infty = T_s$ for the calculation of the temperature at the droplet interface. The heat capacity of the slag was calculated by the weighted average of the heat capacity of the individual oxide species in the slag.

$$C_{p,s} = \sum_{i=1}^n y_i C_{p,i}, \quad [35]$$

where y_i is the wt pct and $C_{p,i}$ is the heat capacity of oxides in the slag. The values of thermal conductivity and heat capacity of steel and slag used for this model are given in Table IV.

2. Macro-kinetics: estimation of total refining rate by the emulsion

The difference between the total weight of impurities (C, Si, Mn, and P) ejected into the emulsion and returning to the bath, as represented by Eq. [7], was calculated at each time step to determine the overall refining rate by the emulsion zone. The total weight of impurities in the ejected metal droplets in the time step, Δt , was determined by estimating the droplet generation rate and the bath concentration as presented in Eq. [8] (Table II). The total mass of impurities (in the droplets) that returns to the bath at time, t , was calculated from the refined concentration, a number of droplets, the weight of droplet, and residence time for all the size groups, described by Eq. [9] (Table II). The number of droplets returning to the bath for a particular size class was calculated from the proportional weight and average size of the droplets in the same size class. In a

particular group, a uniform droplet size of all the ejecting droplets was assumed in the model calculation.

C. Slag–Bulk Metal Zone

Due to the impact force of the top gas jet, the slag formed in the jet impact is likely to be pushed outwardly from the cavity and a region of permanent contact between the slag and metal can establish in the region near to the refractory wall of the vessel. This region was considered as slag–bulk metal zone and the impurities in the hot metal react with the slag to form their respective oxides. The condition of mixed controlled mass transfer was applied to estimate the reaction kinetics at the slag–bulk metal interface. Overall mass transfer coefficient was determined by Eq. [18]. Similar to the jet impact zone, the mass transfer coefficient in the metal phase was calculated by using the correlation suggested by Kitamura *et al.*^[23] as a function of bath geometry, temperature, and stirring energy. The slag side mass transfer coefficient was determined as a function of stirring power and temperature.^[7] The mathematical expressions for the mass transfer correlations are presented in Appendix A.1.

The area of slag–metal (A_{sm}) interface was calculated by subtracting the cavity area from the geometrical area of the bath surface. For non-coalescence cavities, the area of slag–bulk metal interface can be expressed by the following equation:

$$A_{sm} = \pi \left(\frac{D_b^2}{4} - n_n \times r_{cav}^2 \right). \quad [36]$$

Here D_b is the diameter of the bath surface (m); n_n is the number of nozzles in the lance tip; and r_{cav} is the radius of the jet cavity (m).

In this study, the effect of surface oscillation was neglected in the calculation of the interfacial area between slag and bulk metal. The instantaneous equilibrium between the reactants and products was assumed at each computational time step, and the interfacial concentration was determined from the partition ratio correlations described for slag–metal drop interface (Table III). The temperature and the concentration of bulk metal instead of metal droplet were applied in evaluating the interfacial concentration at the slag–bulk metal phase boundary.

D. Dynamic Slag Generation Model

The rate equations for C, Si, Mn, and P described in Table II need the dynamic input of slag oxide compositions to evaluate the kinetic parameters such as interfacial concentration and residence time of metal drops in the emulsion phase. A dynamic slag generation model was coupled with the multi-zone kinetic model for simultaneous estimation of slag and hot metal composition during the blow. Modeling of lime and dolomite dissolution was developed as a function of temperature, slag composition, and stirring intensity as proposed by Dogan *et al.*^[55] The saturation concentration of CaO and MgO was calculated as a function of slag composition and temperature using FactSage 7.1^[56] thermodynamic package and given as dynamic input to the model.

1. Fe₂O generation model

The Fe₂O generation model was developed by the method of oxygen balance inside the converter.^[7] It was assumed that every mole of oxygen injected into the converter was consumed by the chemical reactions. The difference between the mass of oxygen input and the oxygen consumed by oxidation of Si, Mn, P, C, and CO, was used to calculate the oxygen available for iron oxide formation in slag. The weight of oxygen injected into the furnace *via* top blowing and the oxygen contained in the iron ore was considered as model inputs. Oxygen consumption by C, Si, Mn, P, and CO was evaluated from the kinetic models at each time step. Figure 4 shows the schematic of dynamic Fe₂O calculation in slag by the method of oxygen balance. A fixed ratio of FeO/Fe₂O₃ = 0.3 was considered at the slag and hot metal phase boundary.^[57] The total iron oxide (pct Fe_tO) in slag, at a given time step, was estimated from the available oxygen (kg) and the slag weight. The weight of slag was calculated by adding individual oxide components in slag, generated from oxidation reactions and dissolved flux at each computational time step.

The oxygen mass balance equation for the calculation of iron oxide concentration in slag can be expressed by the following equation:

$$\begin{aligned}
 & 0.01 \times \frac{16}{71.5} \times W_s^t \times \frac{d(\text{pct FeO})}{dt} \\
 &= \left(\frac{dW_{O_2}}{dt} + \frac{48}{159.7} \times \frac{dW_{\text{ore}}}{dt} \right) - 0.01 \times \frac{16}{12} W_m^t \\
 &\quad \times (1 - \text{PCR}) \times \frac{d[\text{pct C}]}{dt} - 0.01 \times \frac{16}{12} W_m^t \times \text{PCR} \\
 &\quad \times \frac{d[\text{pct C}]}{dt} - 0.01 \times \frac{32}{28} W_m^t \times \frac{d[\text{pct Si}]}{dt} \\
 &\quad - 0.01 \times \frac{16}{55} W_m^t \times \frac{d[\text{pct Mn}]}{dt} - 0.01 \times \frac{80}{62} W_m^t \\
 &\quad \times \frac{d[\text{pct P}]}{dt} - 0.01 \times W_m^t \times \frac{d[\text{pct O}]_b}{dt},
 \end{aligned} \tag{37}$$

where W_{O_2} is the weight of injected oxygen; W_{ore} is the weight of ore; and PCR denotes the

post-combustion ratio. W_m^t and W_s^t are the hot metal and slag weight, respectively, expressed by Eqs. [38] and [39].

$$W_m^t = W_m^{t-\Delta t} - \Delta W_{m,\text{ref}}^t + \left(\frac{dW_{\text{sc}}^m}{dt} \right) \Delta t + \frac{2M_{\text{Fe}}}{M_{\text{Fe}_2\text{O}_3}} \left(\frac{dW_{\text{ore}}}{dt} \right) \Delta t, \tag{38}$$

$$W_s^t = W_s^{t-\Delta t} + \Delta W_{\text{MOx}} + \left(\frac{dW_L}{dt} \right) \Delta t + \left(\frac{dW_D}{dt} \right) \Delta t, \tag{39}$$

where $\Delta W_{m,\text{ref}}^t$ is the weight of refined hot metal; $\frac{dW_{\text{sc}}^m}{dt}$ is the scrap melting rate; M_{Fe} and $M_{\text{Fe}_2\text{O}_3}$ are the molar mass of iron and iron(III) oxide. In Eq. [39], ΔW_{MOx} is the sum of all the oxide; $\frac{dW_L}{dt}$ and $\frac{dW_D}{dt}$ are the dissolution rate of lime and dolomite, respectively.

In the above calculation, it was assumed that the top gas contains 100 pct oxygen and the iron ore was considered to be pure hematite (Fe₂O₃). The dissolved oxygen concentration in the bulk metal has been calculated from the equilibrium value with the slag ((FeO) = [Fe] + [O]).

E. Post-combustion

As shown in Eq. [37], the estimation of wt pct Fe_tO in the slag needs the quantitative information of how much oxygen consumed by CO to form CO₂. It has been observed that the mechanism of post-combustion in the converter is complex, resulting from heterogeneous chemical reactions occurring in the unsteady state. The dynamic process variables like the change in lance height, scrap characteristics, oxygen flow rate, and the height of slag foaming exert a substantial effect on the PCR.^[58] These variables change rapidly particularly during the initial stage of blowing. Due to the above complexity, a simplified approach was considered in order to investigate the effect of post-combustion on Fe₂O evolution during the blowing process. Two profiles of PCR, based on the observed plant data, were considered in the model calculations. Profile 1, a dynamic PCR profile in which the concentration CO was assumed to change linearly during 0 to 20 and 80 to 100 pct of blowing time.^[59] In profile 2, a constant PCR value of 0.08 was taken throughout the blow. The two different PCR profiles employed in the model calculations are illustrated in Figure 5.

III. COMPUTATION MODEL DEVELOPMENT

For better representation of overall process model and interaction between various phases, the system has been divided into three reaction zones and several sub-models are developed to estimate the thermodynamic and kinetic parameters of refining reactions in each zone. Figure 6 illustrates the schematic of the three reaction zones and the sub-models in each zone. The reaction zones are connected to each other by material and heat flow. Metal

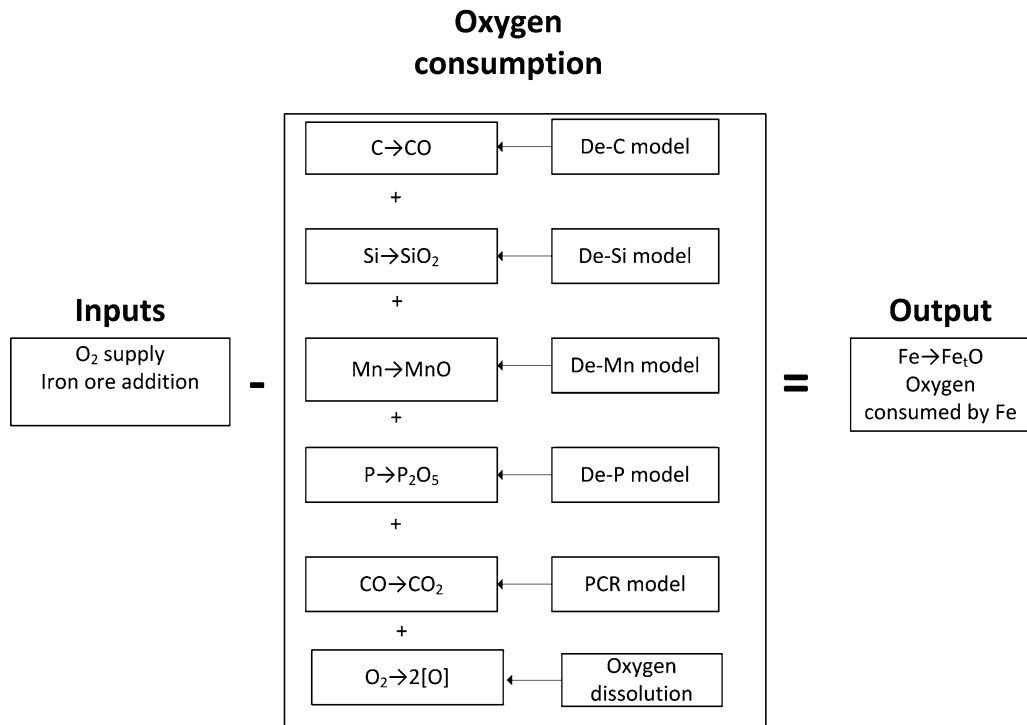


Fig. 4—Model for Fe₂O evolution during blowing period.

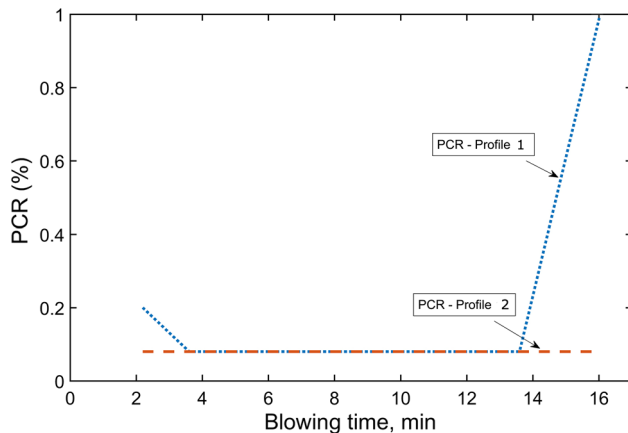


Fig. 5—Post-combustion profile used for Fe₂O generation model (PCR post-combustion ratio).

and slag transfer takes place at jet impact and slag–bulk metal boundary, whereas metal drops and slag transfer takes place between the emulsion and hot metal. The mass flows such as hot metal, scrap, and iron ore are given as input to the hot metal reaction zone. The dynamic parameters such as oxygen flow rate, lance height, bottom blowing rate, and flux addition were given as input to the sub-models in each reaction zone. Each sub-model is built separately and finally connected to each other to simulate the overall process. For example, a droplet generation model was built separately and connected with micro-kinetic model for the droplet to estimate the total rate of refining in emulsion zone.

A. Assumptions

The following assumptions were taken during the formulations of the dynamic model.

- (1) The reactions in the BOF were confined to three primary regions. The possibility of several other reactions such as between the refractory material and slag/metal, reverse emulsification (slag drops inside bulk metal), were ignored in this study.
- (2) A heat balance model to calculate the temperature of metal and slag has not been included in this study. A linear temperature profile, which varies between 1623 K and 1923 K (1350 °C and 1650 °C) during the blowing period, was used for the calculation of hot metal temperature. The slag temperature was considered 100 °C higher than the hot metal temperature.^[5] The authors are aware that a linear temperature profile is simplified assumption, may be ideally suited for the Cicutti's heat data (measured bath temperature varies linearly during the blow). However, in real steelmaking practice, the type and amount of scrap or flux addition practice can have a significant impact on the thermal profile of hot metal, which need to be taken into account in the dynamic model.
- (3) It was assumed that 30 ton of scrap had been melted entirely during first 7 minute of the blow. A linear scrap dissolution rate based on the model result by Dogan *et al.*^[5] was used. The linear melting rate assumption may not be necessarily correct since the melting (and dissolution) of scrap proceeds with the formation of solidified pig iron layer on the top at

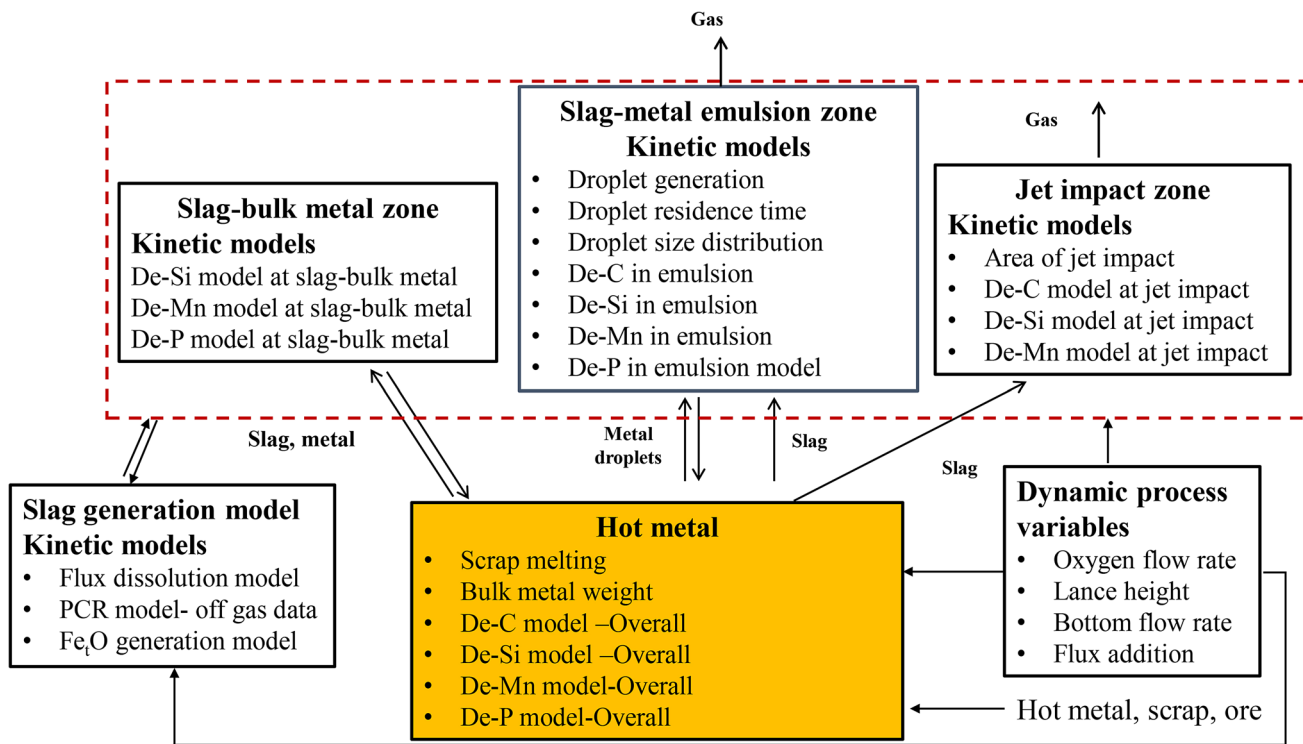


Fig. 6—A three-zone kinetic model for prediction of metal and slag composition during blowing period of a top/combined blowing steelmaking converter process.

the beginning period and it delays the melting process. In the present work, a simplified assumption of rapid melting of the shell is considered to demonstrate the general principle of the multi-zone kinetic model in a BOF process.

- (4) Iron ore was charged into the furnace during the initial stage of furnace operation. It was assumed that the dissolution of iron ore completes during the first 2 minutes of the blow.
- (5) The lime and dolomite particles added into the furnace are assumed to be spherical having diameter 0.045 and 0.03 m, respectively. One ton of lime and 1.7 ton of dolomite were added before the start of the blow. The remaining amount of lime was added in a continuous interval within 7 minutes of the blow. The remaining dolomite was added 7 minutes after the start of the blow.
- (6) The droplets ejected from the melt were assumed as spherical in shape. The angle of inclination of the droplets is assumed 60 deg with respect to the bath surface. In a practical BOF operation, a small fraction of metal fragments are escaped from the mouth of the converter and some are caught by the jet and return to the melt phase. However, in the present model, it was assumed that all the droplets ejected from the melt participate in the reactions in the emulsion zone. The effect of bottom flow rate on droplet generation was ignored in this study.
- (7) While discretizing the continuous process of droplet generation, it was assumed that all the droplets in a given time step Δt are ejected simultaneously at the start of each computational step.

- (8) The motion of metal droplets in the emulsion is influenced by the density and viscosity of the slag-gas continuum. Ito and Fruehan reported that the gas volume fraction in the emulsion varies from 0.7 to 0.9.^[60] The average value of 0.8 has been adopted in the model.

B. Computational Strategy

The numerical program uses explicit finite difference method, which marches forward with time, solving for the bath and slag composition at next time step by using the input parameters calculated in the previous time step. The solution starts at the second time step based on the initial conditions, which were given as an input to the model. The computational platform uses a central model where the calculation of liquid metal concentration, slag composition, slag weight, and hot metal weight takes place and several sub-models to evaluate the transient rate parameters. The central model has been connected in parallel with the sub-models.

Figure 7 demonstrates the flowchart of the computation program of the complete mathematical model. Initially, the value of the global parameters such as constants, properties of slag and metal (e.g., density, molecular weight) were given as input to the model. At the start of the program, the parameters such as slag compositions, metal chemistry, hot metal weight, slag weight, the temperature of metal and slag, have been given as initial inputs to the computational program.

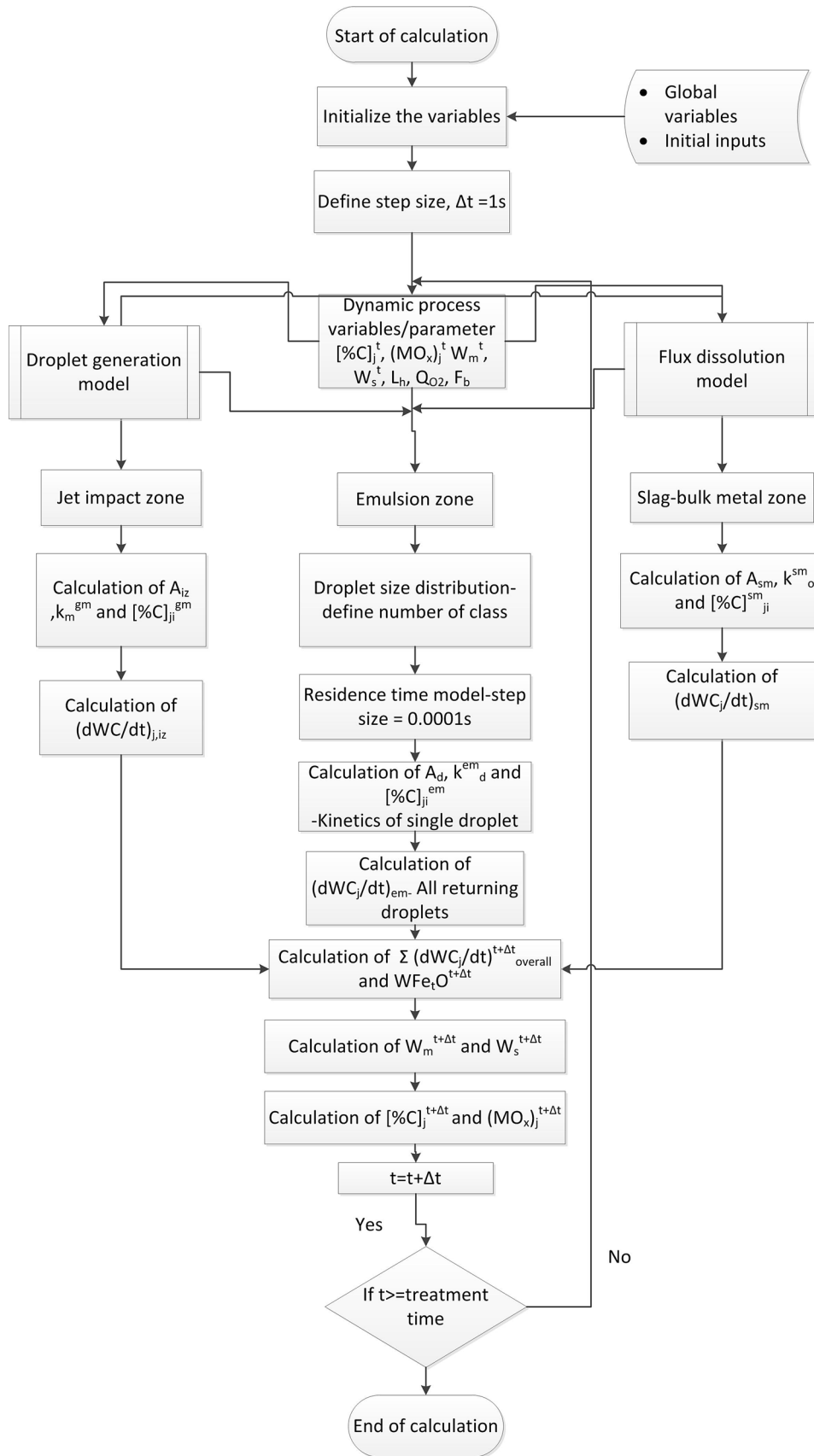


Fig. 7—Algorithm for BOF dynamic model.

The simulation starts after 2.2 minutes available after this time. Once, the step size was selected, the dynamic process variables such as lance height, oxygen flow rate, bottom blowing flow rate were given as input to the model at each time step by predefined functions obtained from converter operation. The flux dissolution models compute the amount of lime and dolomite dissolved in slag at each time based on the dynamic flux addition inputs. The amount of droplet generated from the melt was calculated by the modified droplet generation sub-model and has been used to estimate the total refining by the emulsion zone. In the emulsion zone, a time step of 0.0001 seconds was chosen to calculate the trajectory of metal drops. The rate of refining of hot metal from the different zones was computed at each time step. The overall rate of C, Si, Mn, and P in the previous time step was used to calculate the weight of iron oxide (W_{FeO}) generated at each blowing time. The weight of slag evolution at each time step was evaluated by summing all the oxides of Si, Mn, P, and Fe with the dissolved amount of flux. Once the weight of metal and slag are known, mass balance is performed to predict the wt pct of metal and slag composition at $t + \Delta t$. The calculation continues until the time reaches the total blowing time of BOF operation.

C. Input Data

The initial input and the process parameters used for the model were taken from a 200-ton LD converter studied by Cicutti *et al.*^[45] Table V shows the complete list of parameters used to develop the model. The metal and slag sample in their work was collected from the mouth of the converter by the use of a special sampling device. The initial values of slag and metal compositions were taken as the input to the model. The measured slag

and metal composition at different intervals of blowing time were used to validate of the model predictions. The blowing profiles (both top and bottom) employed in the converter operation were given as dynamic input to the model. The other parameters used for calculating the physicochemical properties of slag, metal, and gas are listed in Table V.

D. Steady-State Solution

To establish the optimal solution, a mathematical convergence analysis was performed for different iterative time steps. Numerical stability of the solution is reached when the solutions for various time steps are

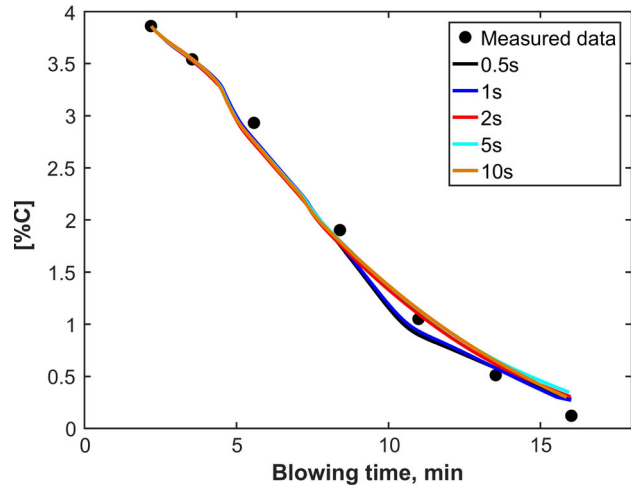


Fig. 8—Model prediction of carbon concentration variation as a function of blowing time with different computational time steps.

Table V. Model Input Parameters

Input Parameters	Values
Initial hot metal composition (blowing time = 2.2 min)	170,000 kg, wt pct C = 3.86, wt pct Si = 0.19, wt pct Mn = 0.29, wt pct P = 0.065
Scrap composition	30,000 kg, wt pct C = 0.08, wt pct Si = 0.001, wt pct Mn = 0.52
Hot metal temperature	1623 K to 1923 K (1350 °C to 1650 °C)
Initial slag composition and weight	initial slag weight at 2.2 min = 5200 kg, total lime added = 7600 kg, iron ore = 1900 kg, quartzite = 800 kg slag composition: wt pct CaO = 27, wt pct FeO = 33, wt pct SiO ₂ = 17, wt pct MnO = 13.5, wt pct MgO = 5, wt pct P ₂ O ₅ = 3.5
Oxygen blow	620 Nm ³ /min, six hole lance
Bottom blow (Ar/N ₂)	2.5 – 8.33 m ³ /min
Lance height	2.5, 2.2, 1.8 m
Steel density	7000 kg/m ³
Slag density	partial molar volume method ^[61]
Surface tension of steel	1.7 N/m
Viscosity of slag	modified Urbain model ^[62]
Diffusion coefficient in metal phase at 1873 K (1600 °C)	C: 2.0×10^{-9} m ² /s, Si: 3.8×10^{-9} m ² /s, Mn: 3.7×10^{-9} m ² /s, P: 4.7×10^{-9} m ² /s
Gas fraction in emulsion	0.8
Diameter of initial droplets	0.00023 to 0.00335 m, 10 classes
Angle of droplet ejection	60 deg

converged. Figure 8 shows the predicted value of carbon concentration in the bath as a function of blowing time for the different values of computation time. The time step (Δt) was varied from 0.5 to 10 seconds and the decarburisation profile was produced for each time step. As shown in Figure 8, when the time step becomes smaller, the solution for 0.5 and 1 seconds was identical, which proves the computational accuracy of the computer program. To reduce the computational time, the time step of 1 second was selected in the present model calculations. The total computation time for the dynamic slag and metal prediction for one blowing period using Matlab© 2016a on a Windows PC having Intel(R) Core(TM) i5-4570 CPU @3.20 GHz with 8 GB RAM is approximately 20 minutes.

IV. MODEL VALIDATION AND DISCUSSIONS

A. Temperature at the Reaction Interfaces

A thermal gradient can exist inside a BOF converter due to the formation of localized reaction zones.

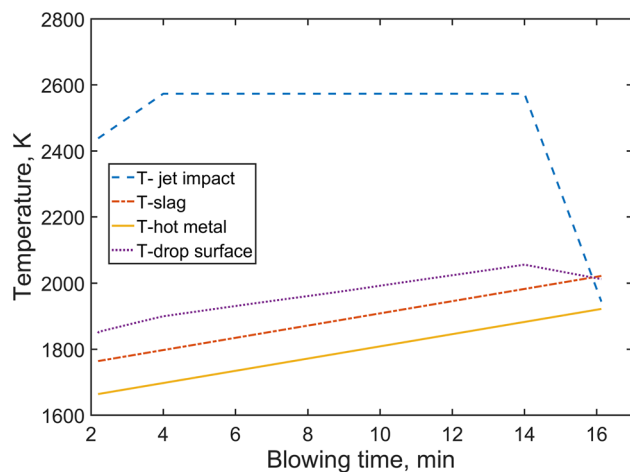


Fig. 9—Temperature change across various reaction interfaces inside the furnace during the blowing time.

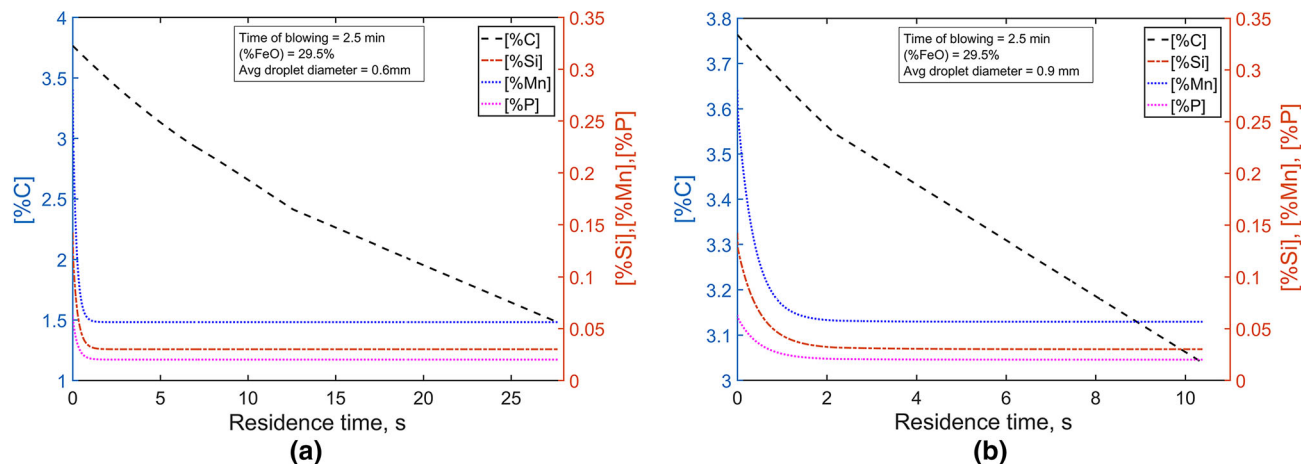


Fig. 10—Removal kinetics of C, Si, Mn, and P of a single metal drop in emulsion: (a) initial droplet diameter = 6×10^{-4} m and (b) initial droplet diameter = 9×10^{-4} m.

Numerous researchers attempted to measure the temperature at different zones of the converter.^[63,64] Chiba *et al.*^[63] reported that the temperature of the hot spot jumps suddenly to 2273 K (2000 °C) at the beginning stage of the blowing, then fluctuates between 2373 K and 2773 K (2100 °C and 2500 °C) during the main blow period, and finally equals to the hot metal temperature. Rote and Flinn observed that the temperature difference between the top surface and the bottom of the vessel varies between 200 and 400 K depending on the blowing type (soft or hard blowing).^[64] Since the temperature is an essential factor in the equilibrium partitioning of refining elements, the model calculations for interfacial temperature in different reaction zones were developed.

In common with Chiba *et al.*, it was assumed the temperature in the hot spot increases linearly from 2273 K to 2573 K (2000 °C and 2300 °C) during the first 25 pct of the blow. During the main blow, between 25 and 80 pct of the blow, the temperature was maintained at a constant value of 2573 K (2300 °C). Finally, the temperature gradient between the hot spot and the liquid bath begins to disappear and hot spot temperature gradually decreases after 80 pct of the blow.^[65] Industrial measurements indicated that the temperature of slag is generally 20 to 100 K hotter than the hot metal during the blowing period.^[66] The temperature difference between the metal and slag was reported to be high during the initial period and the gradient becomes smaller towards the end blow period. In the present work, for the sake of simplicity, the average temperature of the slag was assumed to be 100 K higher than the hot metal temperature.

The surface temperature of the moving droplets in the slag–metal emulsion was calculated by applying Eq. [33]. The variation of temperature in different zones of the converter used in the model is shown in Figure 9. It was observed that the surface temperature of the droplets is 90 to 200 K higher than the metal bath temperature. The temperature profile of droplet surface varies linearly with the blowing time during almost all the part of the blow. Towards the end of the blow, there

is a decreasing trend observed which is due to a reduction in the hot spot temperature as a result of slowing down of the decarburization reaction. It should be acknowledged that the current procedure for estimation of interfacial temperature is based on several simple assumptions and no rigorous heat balance model was applied in the calculation. A dynamic heat balance model focusing on the micro- and macro-kinetics of heat transfer in the recirculated metal drops in the emulsion, coupled with the present multi-zone model, can provide a clear insight into reactions in a BOF process.

B. Kinetics of Refining of Droplet in the Emulsion

The model predictions of the compositional change of two classes of droplets having average diameter 6×10^{-4} m (0.6 mm) and 9×10^{-4} m (0.9 mm) at 2.5 minutes of blowing time are shown in Figure 10. The reaction rates of Si, Mn, and P in the droplet are found to be rapid and reach the state of equilibrium within a few seconds in the emulsion. In the 0.6 mm droplets, the concentrations of Si, Mn, and P approach the equilibrium value within 2 seconds. In contrast, the refining of C continues during the entire 27 seconds of residence in the emulsion phase. It was also observed that the refining rate of droplets, particularly decarburisation, is a function of droplet size. The droplets in the lower region of size spectrum exhibit high efficiency of refining and make a greater contribution to the

conversion process of Si, C, Mn, and P during the reaction in the emulsion. About ~60 pct of decarburization was observed for 0.6 mm droplet in contrast to ~18 pct when the droplet size was increased by 0.3 mm. This may be due to a shorter reaction time (~10 seconds) of 0.9-mm-diameter droplet as compared to 0.6 mm droplets (~27 seconds). Here the extent of decarburisation reaction is limited by the time of residence of droplet in emulsion. The model prediction of the droplet refining kinetics has been found to be consistent with the observed refining of metal drops reported by IMPHOS pilot plant experiments.^[18] The measurements of droplet composition collected from the emulsion sample show a high depletion of Mn, P, and Si, but the C concentration is more than 1 wt pct during the initial blowing period. The rapid removal rates of Si, Mn, and P during the opening stage of oxygen blow are thought to be the result of high thermodynamic driving force and large surface area created by small-sized metal drops in the emulsion.

C. Validation

The variation of bath concentration was simulated by the three-zone kinetic model with the dynamic change of process variables for a 200-ton LD-LBE converter. Figure 11 illustrates the simulated profiles of C, Si, Mn, and P as a function of blowing time for the predefined PCR profiles. As shown in the figure, the model

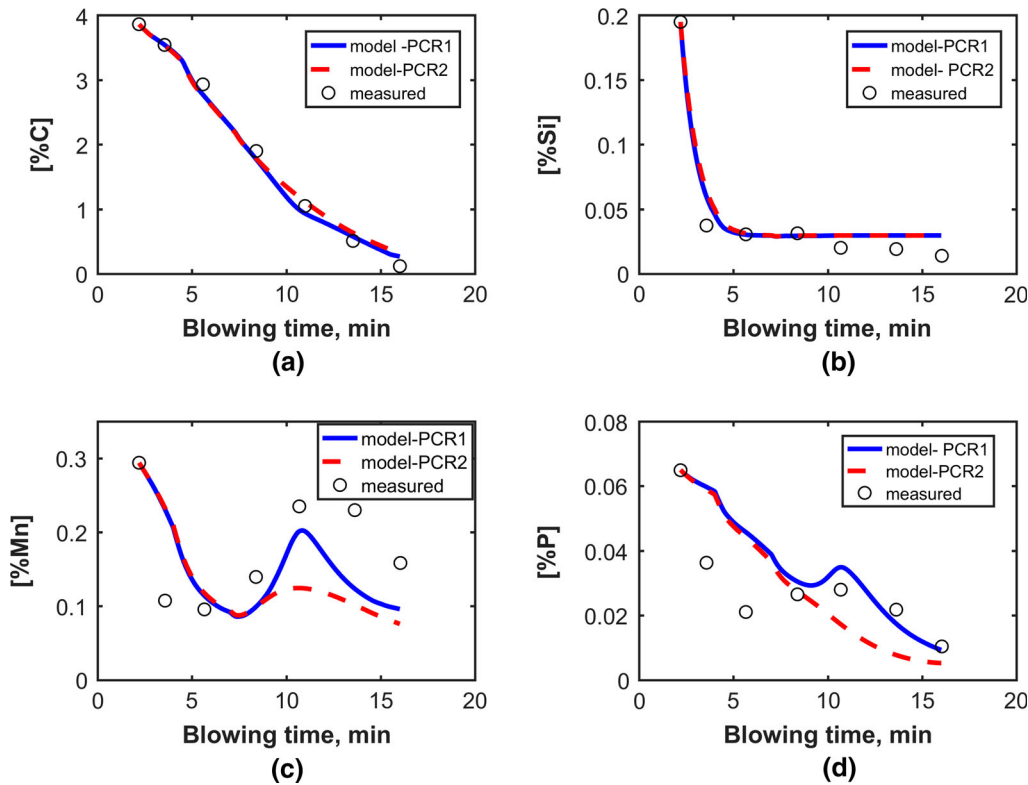


Fig. 11—Model prediction of hot metal composition (wt pct) during the blowing period: (a) carbon, (b) silicon, (c) manganese, and (d) phosphorus.

predictions of bath composition with PCR profile 1 agree well with the measured solute concentration during different intervals of the blowing period. It was observed that changing the PCR does not have much influence on the predictions of C and Si, albeit the reversion behavior of Mn and P is highly influenced by PCR. This is most likely due to the strong dependence of the equilibrium concentrations of Mn and P on the change of slag chemistry (slag Fe_tO), which in turn is controlled by the amount of oxygen consumed in the process of post-combustion reaction.

The model prediction of decarburization has been found to be in excellent agreement with the plant data. The three distinct regions of decarburization profile, commonly observed in a BOF process, were distinguished in the model prediction. The Si refining predicted by the model was found to be consistent with the measured values. As reported in the previous publication, the refining of Si can be explained by a three-zone approach where a significant fraction of refining is observed to take place by the droplet mechanism.^[27] In the case of Mn removal, the high rate at the beginning of the blow, reversion during the middle of the blow, and again an increase in rate towards the end blow were

captured by the model. It was observed that the oxidation and reversion of Mn from slag to metal is primarily caused by the droplet recirculation by the emulsion zone. The equilibrium concentration of Mn at the metal drop–slag interface, which is strongly dependent on temperature and slag chemistry, was found to be the deciding factor for reversion of Mn. The details about the mechanism of Mn refining and the role of different reaction zones on the rate will be discussed separately.^[21] The rate of P refining predicted by the model shows a similar oxidation and reversion behavior as Mn. The reversion of P predicted by the model shows a similar behavior as the actual process. However, a slow removal rate of P as compared to the actual process was noticed. The mismatch between the Mn and P predictions may be caused by the error in the evaluation of rate parameters and the estimation of equilibrium concentration at the metal drop and slag interface. An increase in the slag–bulk metal interfacial area as a result of surface oscillation could be another reason for the deviation. Further experimental work on the reaction kinetic study of Fe–C–Si–Mn–P drops in steelmaking slag is essential to evaluate the kinetic parameters associated with the simultaneous oxidation/reduction reactions.

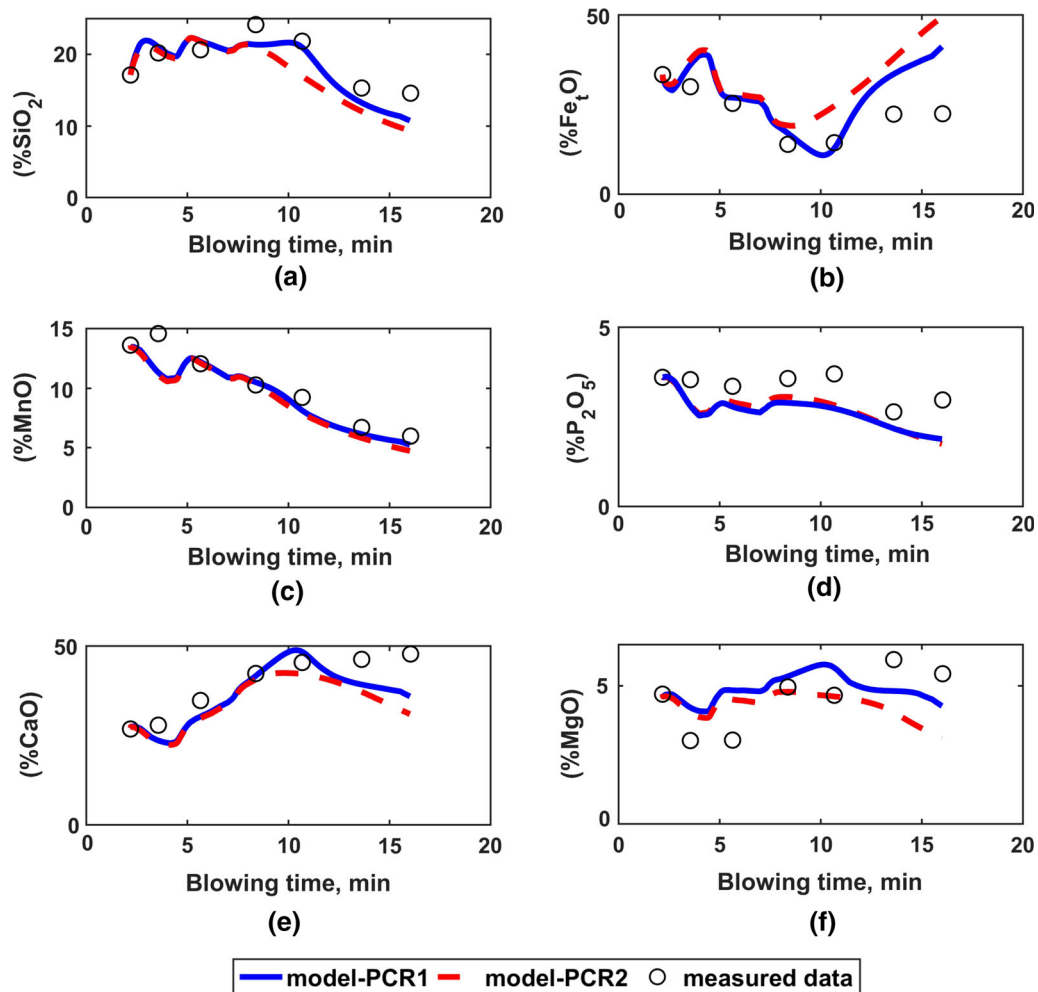


Fig. 12—Evolution of slag composition (wt pct) during blowing period. (a) SiO₂, (b) Fe_tO, (c) MnO, (d) P₂O₅, (e) CaO, (f) MgO.

The evolution of slag during the blowing process for the predefined two post-combustion profiles is illustrated in Figure 12, and the results are compared with the measured slag data. As shown in the figure, the concentration of oxides in the slag is inconsistent with the measured values in both the PCR profiles. However, it can be noticed that the level of Fe_2O is sensitive to the oxygen consumed by post-combustion reaction. The PCR profile 1 where a dynamic PCR was adopted has been found to produce better results for Fe_2O prediction than a constant PCR. During the initial part of the blow, *i.e.*, after 1 minute from the start of computation, the weight of Fe_2O was found to increase with time. It might be due to the slow decarburization rate and Fe_2O was not consumed entirely during the initial stage. After approximately 5 minutes of the start of the blow, the Fe_2O percentage starts to decrease because the rapid rate of decarburization begins to take place and Fe_2O was largely consumed by carbon. Until 10 minutes or so, Fe_2O reaches the lowest value and after that, it increases due to decrease in hot metal weight in the emulsion phase. This results in slowing down of the Fe_2O consumption rate by the droplets. A deviation of Fe_2O between the model and the measured value was observed during the end blow period. In the present calculation of Fe_2O , when the impurity level reaches to the low level, virtually all the injected oxygen ends up in forming iron oxide and thus a sharp rise in slag iron oxide was observed. The kinetics of Fe_2O formation with regard to saturation of Fe_2O (the equilibrium driving force of FeO between the bulk and interface) in slag and the loss of Fe as dust were not considered in the present work. Also an inaccuracy in PCR may introduce some error in oxygen balance equation. The above factors may be responsible for the deviation observed in the simulated iron oxide profile, particularly during initial and end blow period. Due to the overestimation of Fe_2O in the end blow period, the model prediction of slag weight and CaO concentration finds some deviation from the measured values.

The evolution of hot metal weight and the slag during the blowing period for PCR 1 profile is shown in Figure 13. The change in the weight of the melt is

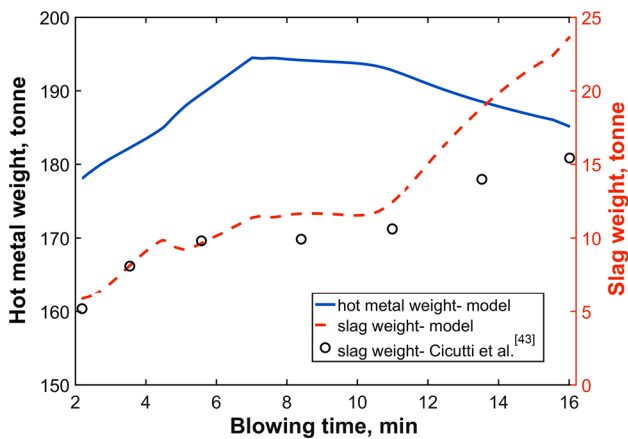


Fig. 13—Variation of hot metal and slag weight during the blowing period as predicted by the model for PCR profile 1.

calculated using the amount of scrap melted, the amount of droplet generated, and fall back and the weight of metal loss by forming slag during time step Δt . It can be observed that the weight of the hot metal increases gradually due to the gradual melting of the scrap until 7 minutes of the blow. After this period, the bulk metal weight decreases till the end of blow due to oxidation loss of various impurities from the melt. Similarly, the weight of slag increases initially due to the dissolution of lime and dolomite continuously. The deviation of slag weight after 10 minutes of the blow is due to the overestimation of Fe_2O calculated by the model.

It should be acknowledged that the current study does not include the effect of bottom blowing on droplet generation. While there is evidence that bottom blowing affects the droplet generation rate in a combined blowing converter, none of the predictive models yet incorporated the bottom blowing effect on the estimation of the droplet generation rate in oxygen steelmaking process. Due to unavailability of quantified models, the authors have ignored the effect of bottom blowing in the present work.

V. CONCLUSIONS

A three-zone kinetic model has been developed to predict the metal and slag compositions during the BOF process. The converter was divided into three reaction zones, and kinetics of refining in each zone has been estimated by providing mathematical treatment to the physicochemical process occurring in different zones of the converter. The fundamental understanding of BOF process such as bloating and refining of metal droplets in the slag–metal emulsion and the reaction taking place in the jet impact zone and slag–bulk metal region were successfully incorporated into the mathematical model. A Fe_2O generation model was developed and coupled with the kinetic model for simultaneous prediction of slag and metal during the blowing process. The following conclusion can be made based on the present study.

- (1) A multi-zone kinetic model can be useful to simulate the reactors where the reactions occur with multiple interfaces with transient rate parameters. In the BOF process, it is evident that the overall kinetics can be successfully simulated by a multiple zone reaction approach by use of time variant rate parameters as a function of process dynamics.
- (2) The model predicts that the significant share of refining in a BOF process is caused by the recirculation of metal fragments through the emulsion zone. The number of metal droplets ejected, size and time of residence of droplets in the emulsion, and the equilibrium concentration at the interface of the droplet are the primary factors that decide the refining kinetics in the emulsion phase. The large thermodynamic driving force of droplets during the initial stage of blowing is responsible for high refining rate of Si, Mn, and P.

- (3) It is predicted that the reaction rates of Si, Mn, and P refining in the droplet are fast and approaches equilibrium within a few seconds inside the emulsion. The oxidation rate of C is influenced by the initial droplet size.
- (4) The metal drops in the lower region of size spectrum make a significant contribution to the conversion process in the emulsion zone.
- (5) The formation of Fe_tO in the slag is highly inter-linked with the PCR. A dynamic post-combustion model, particularly during the early and end blow period is useful for accurate prediction of Fe_tO evolution in slag.

We recommend that experimental work on studying the detailed kinetics of the reactions of Fe-C-Si-Mn-P in an oxidizing slag will provide greater knowledge on the kinetics of steelmaking process. Future work on developing a heat balance model, focusing on evaluating the macroscopic heat transfer of recirculating metal drops, and coupling with the present kinetic model can provide a detailed insight into the BOF reactions.

ACKNOWLEDGMENTS

The authors wish to acknowledge the financial support provided by Tata Steel to carry out this research work. BKR would like to thank Mariana Adderley for the constructive and helpful discussion regarding this work.

APPENDIX

A.1 Mass Transfer Coefficient in Hot Metal and Slag

The mass transfer coefficient in the hot metal has been calculated by the following relationship,^[23]

$$\log k_m = 1.98 + 0.5 \log \left(\frac{\varepsilon H^2}{100L} \right) - \frac{125,000}{2.3RT}, \quad [40]$$

where k_m is the mass transfer coefficient in metal phase (cm/s); ε is the stirring energy (W/t); H and L are the bath depth (cm) and diameter of the furnace, respectively; and T is the temperature in the impact zone (K). The total stirring energy was calculated by using the combined effect of the top and bottom gas injection in the BOF.^[67]

The slag phase mass transfer coefficient was given by^[7]:

$$k_s = a \exp \left(-\frac{37,000}{RT} \right) \cdot \varepsilon^b, \quad [41]$$

where k_s is the mass transfer coefficient in slag phase (cm/s); R gas constant (J mol⁻¹ K⁻¹); and a and b are the empirical parameters, assumed to be 1.7 and 0.25, respectively.^[7]

A.2 Calculation of Cavity Height and Radius

The height and radius of the individual cavity formed by the top jet can be expressed as follows:

$$h = 4.469 \dot{M}_h^{0.66} L_h, \quad [42]$$

$$r_{\text{cav}} = 0.5 \times 2.813 L_h \dot{M}_d^{0.282}, \quad [43]$$

where L_h is the lance height (m) and the dimensionless momentum flow rate and is defined as

$$\dot{M}_h = \frac{\dot{m}_n \cos(\text{nangle})}{\rho_m g L_h^3}, \quad [44]$$

$$\dot{M}_d = \frac{\dot{m}_i(1+\sin(\text{nangle}))}{g \rho_m L_h^3}, \quad [45]$$

where \dot{m}_n is the momentum flow rate of the each nozzle, which is related to the total momentum flow rate, \dot{m}_i by the following equations:

$$\dot{m}_n = \frac{\dot{m}_i}{n_n}. \quad [46]$$

Total momentum flow rate:

$$\dot{m}_i = 0.7854 \times 10^5 \times n_n \times d_{\text{th}}^2 \times P_a \left(\frac{1.27P_0}{P_a} - 1 \right), \quad [47]$$

where n_n is the number of nozzles in the lance tip; nangle is the nozzle angle (rad); d_{th} is the throat diameter of the lance (m); P_0 is the top supply pressure (Pa); and P_a is the ambient pressure (Pa).

A.3 Calculation of Equilibrium Distribution Ratios

1. Silicon distribution ratio^[42]

$$L_{\text{Si}} = \begin{cases} 1 - \frac{(\text{pct FeO})}{40}, & (\text{pct FeO}) \leq 40, \\ 0, & (\text{pct FeO}) > 40. \end{cases} \quad [48]$$

2. Manganese distribution ratio^[43]:

$$\begin{aligned} \log k'_{\text{Mn}} = & -0.0180[(\text{wt pct CaO}) + 0.23(\text{wt pct MgO}) \\ & + 0.28(\text{wt pct Fe}_t\text{O}) - 0.98(\text{wt pct SiO}_2) \\ & - 0.08(\text{wt pct P}_2\text{O}_5)] + \frac{7300}{T} - 2.697, \end{aligned} \quad [49]$$

where the apparent equilibrium constant k'_{Mn} is defined as follows

$$k'_{\text{Mn}} = \frac{(\text{wt pct MnO})}{(\text{wt pct T} \cdot \text{Fe}) \times [\text{wt pct Mn}]} = \frac{L_{\text{Mn}} \times \frac{M_{\text{Mn}}}{M_{\text{MnO}}}}{(\text{wt pct T} \cdot \text{Fe})}. \quad [50]$$

T. Fe denotes total Fe and M_{Mn} and M_{MnO} are the molar mass (g/mol) of Mn and MnO, respectively.

3. Phosphorus distribution ratio

The phosphorus equilibrium distribution ratio at the slag–metal interface can be written as^[68] follows:

$$L_p = \frac{K_p f_p h_o^{2.5}}{C \gamma_{PO_{2.5}}}, \quad [51]$$

where K_p is the equilibrium constant; f_p is the activity coefficient of P; h_o is the Henrian activity of oxygen; C is the conversion factor which related (pct P) with the mole fraction of $PO_{2.5}$; and $\gamma_{PO_{2.5}}$ is the activity coefficient of $PO_{2.5}$.

The equilibrium constant for the phosphorus oxidation reaction can be expressed as^[63]

$$\log(K_p) = \frac{17,060}{T} - 8.51. \quad [52]$$

Here h_o is the Henrian activity of oxygen, determined by assuming FeO–O equilibrium.

$$h_o = \frac{\gamma_{FeO}}{X_{FeO} K_F}. \quad [53]$$

K_F is the equilibrium constant for reaction $[Fe] + [O] = (FeO)$, $\Delta G^\circ = -128,090 + 57.99 T$.^[63] γ_{FeO} and $\gamma_{PO_{2.5}}$ are the activity coefficients of FeO and $PO_{2.5}$, determined by Regular solution model proposed by Ban-Ya.^[40] Henrian activity coefficient f_p was determined by employing the first-order interaction parameter. $\log(f_p) = e_p^p [\text{pct P}] + e_p^c [\text{pct C}]$, where $e_p^p = 0.063$ and $e_p^c = 0.19$.^[7]

LIST OF SYMBOLS AND ABBREVIATIONS

A	Interfacial area (m^2)
C_{jm}	Concentration of j th component in metal, $j = \text{Si, C, Mn, and P}$ (wt pct)
C_{ji}	Concentration of j th component on the reaction interface (wt pct)
C_{jd}^{return}	Concentration of j th component of refining droplets (wt pct)
$C_{p,m}$	Heat capacity of bulk metal (J/kg)
$C_{p,s}$	Heat capacity of slag (J/kg)
d_p	Diameter of the droplet (m)
D	Diffusion coefficient of slag (m^2/s)
$F_{G,T}$	Temperature-corrected oxygen flow rate (Nm^3/min)
h	Height of the cavity (m)
k_a	Apparent rate constant ($\text{mol}/m^2 \text{ s atm}$)
k_g	Gas phase mass transfer coefficient ($\text{mole}/m^2 \text{ s atm}$)
k_d^{em}	Overall mass transfer coefficient of droplet (m/s)
k_{jm}^d	Mass transfer coefficient in metal side of droplet (m/s)
k_s^d	Mass transfer coefficient in slag side of droplet (m/s)
k_m^{sm}	Overall mass transfer coefficient at slag–bulk metal interface (m/s)
k_{gm}^m	Mass transfer coefficient in the melt in jet impact area (m/s)

L_h	Lance height (between lance tip and bath surface) (m)
m_d	Mass of a single droplet (kg)
$m_{d,p}$	Average mass of droplets belongs to p th size class (kg)
m_d^{return}	Weight of a single droplet returns to the bath (kg)
M	Molecular weight (g/mol)
$N_p^{\text{eject},t}$	Number of droplets of p th class size ejects to the bath at blowing time t (–)
$N_p^{\text{return},t}$	Number of droplets of p th class size returns to the bath at blowing time t (–)
$N_{B,T}$	Modified blowing number (–)
$P_{CO_2}^b$	Partial pressure of CO_2 (atm)
$P_{O_2}^b$	Partial pressure of O_2 (atm)
PCR	Post-combustion ratio (–)
Re	Reynolds number (–)
$R_{B,T}$	Droplet generation rate (kg/min)
Sh	Sherwood number (–)
Sc	Schmidt number (–)
r_c	Decarburization rate of the droplet (wt pct/s)
r_c^*	Critical decarburization for bloating (wt pct/s)
r_{cav}	Cavity radius (m)
t_c	Contact time between the metal droplet and slag (seconds)
t_{res}	Residence time of droplet in emulsion (seconds)
T_s	Interface temperature at slag–metal (K)
T_∞	Temperature in the emulsion medium (K)
T_0	Initial temperature of the metal drop at the time of ejection (K)
u	Velocity of the droplet (m/s)
V_d	Volume of droplet (m^3)
W_c	Weight of carbon (kg)
WC_j	Weight of impurity (kg)
W_D	Weight of dolomite (kg)
$W_{d,p}$	Weight proportion of droplet belongs to p th size class (kg)
W_L	Weight of lime (kg)
W_m	Weight of hot metal (kg)
$\Delta W_{m,ref}^t$	Weight of refining hot metal in a numerical time step (kg)
ΔW_{MOx}	Sum of oxide mass in a numerical time step (kg)
W_s	Weight of slag (kg)
W_{jm}^{eject}	Weight of j th element in the hot metal ejected to the emulsion (kg)
W_{jm}^{return}	Weight of j th element in the hot metal return to the bath (kg)
W_{sc}^m	Weight of the melted scrap (kg)

GREEK SYMBOLS

ρ_d	Density of droplet (kg/m^3)
$\rho_{d,0}$	Initial density of droplet (kg/m^3)
ρ_m	Density of the bulk metal (kg/m^3)
ρ_s	Density of slag (kg/m^3)
λ_m	Thermal conductivity of liquid metal (W/m K)
λ_s	Thermal conductivity of slag (W/m K)

SUBSCRIPTS AND SUPERSSCRIPTS

cav	Cavity
d	Droplet
m	Hot metal
<i>P</i>	Number of classes in the droplet size spectrum
eq	Equilibrium
hs	Hot spot
iz	Impact zone
em	Emulsion
sm	Slag/metal
gm	Gas/metal

REFERENCES

- W. Knoop, B. Deo, A. Snoeijer, G. Unen, and R. Boom: *Proc. 4th Int. Conf. Molten Slags Fluxes, ISIJ*, Tokyo, 1992, pp. 302–07.
- H. Jalkanen and L. Holappa: *VII Int. Conf. Molten Slags Fluxes Salts*, The South African Institute of Mining and Metallurgy, 2004, pp. 71–76.
- A.K. Shukla, B. Deo, S. Millman, B. Snoeijer, A. Overbosch, and A. Kapilashrami: *Steel Res. Int.*, 2010, vol. 81, pp. 940–48.
- I.H. Jung, P. Hudon, M.A. Van Ende, and W.Y. Kim: *AISTech Iron Steel Technol. Conf. Proc.*, 2014, vol. 1, pp. 1257–68.
- N. Dogan, G.A. Brooks, and M.A. Rhamdhani: *ISIJ Int.*, 2011, vol. 51, pp. 1086–92.
- F. Pahlevani, S. Kitamura, H. Shibata, and N. Maruoka: *Steel Res. Int.*, 2010, vol. 81, pp. 617–22.
- Y. Ogasawara, Y. Miki, Y. Uchida, and N. Kikuchi: *ISIJ Int.*, 2013, vol. 53, pp. 1786–93.
- R. Sarkar, P. Gupta, S. Basu, and N.B. Ballal: *Metall. Mater. Trans. B*, 2015, vol. 46B, pp. 961–76.
- C. Kattenbelt and B. Roffel: *Metall. Mater. Trans. B*, 2008, vol. 39B, pp. 764–69.
- Y. Lytvyniuk, J. Schenk, M. Hiebler, and A. Sormann: *Steel Res. Int.*, 2014, vol. 85, pp. 537–43.
- D. Guo, D. Swickard, and J. Bradley: *Iron Steel Technol.*, April 2014, pp. 131–40.
- G. Li, B. Wang, Q. Liu, X. Tian, R. Zhu, L. Hu, and G. Cheng: *Int. J. Miner. Metall. Mater.*, 2010, vol. 17, pp. 715–22.
- N. Sasaki, G. Brooks, and M.A. Rhamdhani: *Asia Steel*, Yokohama, Japan, 2015.
- S. Kitamura: *Steel Res. Int.*, 2010, vol. 81, pp. 766–71.
- S. Ohguchi, D.G.C. Robertson, B. Deo, P. Grieveson, and J.H.E. Jeffes: *Ironmak. Steelmak.*, 1984, vol. 11, pp. 202–13.
- G.A. Brooks, M.A. Rhamdhani, K.S. Coley, D. Subagyo, and Y. Pan: *Metall. Mater. Trans. B*, 2009, vol. 40B, pp. 353–62.
- A.K. Hewage, B.K. Rout, G. Brooks, and J. Naser: *Ironmak. Steelmak.*, 2016, vol. 43, pp. 358–70.
- M.S. Millman, A. Kapilashrami, M. Bramming, and D. Malmberg: *IMPHOS: Improving Phosphorus Refining*, European Union, Luxembourg, 2011.
- B.K. Rout, G.A. Brooks, Z. Li, and M.A. Rhamdhani: *AISTech Iron Steel Technol. Conf. Proc.*, 2015, vol. 3, pp. 3225–37.
- B.K. Rout, G. Brooks, M.A. Rhamdhani, Z. Li, F.N.H. Schrama, and A. Overbosch: *Metall. Mater. Trans. B* (submitted, E-TP-17-603-B), 2017.
- B.K. Rout, G. Brooks, M.A. Rhamdhani, Z. Li, F. Schrama, and W. van der Knoop: *Metall. Mater. Trans. B* (submitted, E-TP-17-604-B), 2017.
- Q. Li, M. Li, S. Kuang, and Z. Zou: *Metall. Mater. Trans. B.*, 2015, vol. 46B, pp. 1494–1509.
- S. Kitamura, T. Kitamura, K. Shibata, Y. Mizukami, S. Mukawa, and J. Nakagawa: *ISIJ Int.*, 1991, vol. 31, pp. 1322–28.
- N. Dogan, G.A. Brooks, and M.A. Rhamdhani: *ISIJ Int.*, 2011, vol. 51, pp. 1102–09.
- K. Chou, U.B. Pal, and R.G. Reddy: *ISIJ Int.*, 1993, vol. 33, pp. 862–68.
- B. Deo and R. Boom: *Fundamentals of Steelmaking Metallurgy*, Prentice Hall, Hertfordshire, 1993, p. 194.
- B.K. Rout, G.A. Brooks, Z. Li, and M.A. Rhamdhani: *AISTech Iron Steel Technol. Conf. Proc.*, 2016, vol. 1, pp. 1019–26.
- F.R. Cheslak, J.A. Nicholls, and M. Sichel: *J. Fluid Mech.*, 1969, vol. 36, pp. 55–63.
- S.C. Koria and K.W. Lange: *Steel Res.*, 1987, vol. 58, pp. 421–26.
- P. Kozakevitch: *J. Met.*, 1968, vol. 22, pp. 57–67.
- H.W. Meyer, W.F. Porter, G.C. Smith, and J. Szekely: *J. Met.*, 1968, vol. 20, pp. 35–42.
- G. Brooks, Y.H. Pan, D. Subagyo, and K. Coley: *Metall. Mater. Trans. B*, 2005, vol. 36B, pp. 525–35.
- C.L. Molloseau and R.J. Fruehan: *Metall. Mater. Trans. B*, 2002, vol. 33B, pp. 335–44.
- H. Gaye and P.V. Riboud: *Metall. Trans. B*, 1977, vol. 8, pp. 409–15.
- P. Kozakevitch, G.H. Geiger, M. Olette, and P.V. Riboud: *BOF Steelmaking*, Iron and Steel Society, 1975, vol. 2, Chapter V, pp. 287–88.
- K. Gu, N. Dogan, and K.S. Coley: *Metall. Mater. Trans. B*, 2017, pp. 1–18.
- H. Sun and G. Zhang: *AISTech Iron and Steel Technology Conference Proceedings*, 2005, pp. 257–68.
- K. Gu, N. Dogan, and K.S. Coley: *Metall. Mater. Trans. B*, 2017, vol. 48B, pp. 2343–53.
- F.D. Richardson: *Physical Chemistry of Melts in Metallurgy Academic (Elsevier)*, 1974, vol. 2, pp. 412–16.
- F. Oeters: *Metallurgy of Steelmaking*, Verlag Stahleisen, 1994, pp. 369.
- C.P. Manning and R.J. Fruehan: *Metall. Trans. B*, 2013, vol. 44B, pp. 37–44.
- S. Ban-Ya: *ISIJ Int.*, 1993, vol. 33, pp. 2–11.
- K. Narita, T. Makino, H. Matsumoto, A. Hikosaka, and J. Katsuda: *Tetsu-to-Hagane*, 1983, vol. 69, pp. 1722–29.
- H. Suito and R. Inoue: *ISIJ Int.*, 1995, vol. 35, pp. 266–71.
- C. Cicutti, M. Valdez, T. Pérez, J. Petroni, A. Gómez, R. Donayo, and L. Ferro: *Sixth Int. Conf. Molten Slags, Fluxes Salts*, ISS, Stockholm, 2000.
- S.C. Koria and K.W. Lange: *Metall. Trans. B*, 1984, vol. 15, pp. 109–16.
- B.K. Rout, G.A. Brooks, M.A. Rhamdhani, and Z. Li: *Metall. Mater. Trans. B*, 2016, vol. 47B, pp. 3350–61.
- D. Subagyo, G. Brooks, K.S. Coley, and G.A. Irons: *ISIJ Int.*, 2003, vol. 43, pp. 983–89.
- D. Subagyo, G. Brooks, and K. Coley: *Can. Metall. Q.*, 2005, vol. 44, pp. 119–29.
- Y. Doh, P. Chapelle, A. Jardy, G. Djambazov, K. Pericleous, G. Ghazal, and P. Gardin: *Metall. Mater. Trans. B*, 2013, vol. 44B, pp. 653–70.
- B.T. Chao: *J. Heat Transf.*, 1969, vol. 91, pp. 273–80.
- P. Sulasalmi, V. Ville-Valteri, A. Kärnä, M. Järvinen, S. Ollila, and T. Fabritius: *Metall. Mater. Trans. B*, 2016, vol. 47B, pp. 3544–56.
- T. Nishi, H. Shibata, Y. Waseda, and H. Ohta: *Metall. Mater. Trans. A*, 2003, vol. 34A, pp. 2801–07.
- K. Nishioka, T. Maeda, and M. Shimizu: *ISIJ Int.*, 2006, vol. 46, pp. 427–33.
- N. Dogan, G.A. Brooks, and M.A. Rhamdhani: *ISIJ Int.*, 2009, vol. 49, pp. 1474–82.
- <http://www.factsage.com/>.
- E. Schürmann, K. Obst, L. Fiege, and H. Kaiser: *Steel Res. Int.*, 1985, vol. 56, pp. 425–31.
- M. Hirai, R. Tsujino, T. Mukai, T. Harada, and M. Omori: *Trans. ISIJ*, 1987, vol. 27, pp. 805–13.
- S. Li, X. Wei, and L. Yu: *Fuel*, 2011, vol. 90, pp. 1350–60.
- K. Ito and R.J. Fruehan: *Metall. Trans. B*, 1989, vol. 20, pp. 509–14.
- Slag Atlas*, Verlag Stahleisen GmbH, Düsseldorf, 1995, pp. 345–46.
- A. Kondratiev and E. Jak: *Metall. Mater. Trans. B*, 2001, vol. 32B, pp. 1015–25.
- K. Chiba, A. Ono, M. Saeki, M. Yamauchi, M. Kanamoto, and T. Ohno: *Ironmak. Steelmak.*, 1993, vol. 20, pp. 215–20.
- F.E. Rote and R.A. Flinn: *Metall. Trans.*, 1972, vol. 3, pp. 1373–84.
- Y.E. Lee and L. Kolbeinsen: *ISIJ Int.*, 2007, vol. 47, pp. 764–65.
- M. Ishiguro: *Tetsu-to-Hagane*, 1971, vol. 57, pp. 267–70.
- S.C. Koria and K.W. Lange: *Steel Res.*, 1987, vol. 58, pp. 421–26.
- S. Ban-Ya: *ISIJ Int.*, 1993, vol. 33, pp. 2–11.